Restricting the parameter space of type-II two-Higgs-doublet models with *CP* violation

Mariana Frank,[1,*] Eric Gyabeng Fuakye,[2,†] and Manuel Toharia[3,‡]

[1]*Department of Physics, Concordia University, 7141 Sherbrooke St. West, Montreal, Quebec H4B 1R6, Canada*

[2]*Department of Physics, University of Regina, 3737 Wascana Pkwy, Regina, Saskatchewan S4S 0A2, Canada*

[3]*Department of Physics, Dawson College, 3040 Sherbrooke St. West, Montreal, Quebec H3Z 1A4, Canada*

(Received 10 January 2022; accepted 19 July 2022; published 10 August 2022)

We explore the parameter space of the type-II two-Higgs-doublet model with softly broken Z_2 symmetry, allowing for *CP* violation in the scalar potential. Imposing theory-motivated and experimentally-driven constraints, we show that as the *CP*-violating phases are increased, only small regions of parameter space survive, including regions slightly away from the alignment limit. Electroweak oblique parameters and electric dipole moments emerge as most restrictive constraints. We show that imposing these constraints (as well as theoretical bounds such as perturbativity) the masses of the charged and heavy neutral Higgs, unlike in the *CP* conserving case, are bound from above and below. In particular, the heavy neutral Higgs masses are almost degenerate. In this parameter space region we highlight the relevant decay signals of the heavy neutral Higgs, involving both Zh and WW/ZZ, indicative of *CP* violation in the model.

DOI: 10.1103/PhysRevD.106.035010

I. INTRODUCTION AND MOTIVATION

Our present day knowledge of particle physics, which seeks to address the fundamental building blocks of matter and how they interact, is encapsulated in the Standard Model (SM). The Standard Model is a relativistic quantum field theory based on $SU(3)_C \otimes SU(2)_L \otimes U(1)_Y$ gauge symmetry, where the group $SU(2)_L \otimes U(1)_Y$ is responsible for electroweak unification, and $SU(3)_C$ provides the description of strong interactions [1–5]. In 2012, the LHC discovered a spin-0 scalar boson with mass about 125–126 GeV [6,7], and with properties in remarkable agreement with the Higgs boson predicted by the SM, was especially important, as it confirmed experimentally one of the key mechanisms of the SM, responsible for giving masses to the SM particles. The dynamics of this mechanism, known as electroweak symmetry breaking (EWSB), can have a significant effect on the properties of SM particles. Unfortunately, despite its remarkable success, the SM cannot be the ultimate theory. Experimentally, it lacks a dark matter candidate, a mechanism for neutrino masses and mixing (neutrino oscillations) or for sufficient generation of matter-antimatter asymmetry, to name a few. From a theoretical point of view, despite being the most successful model to date, the SM is inherently an incomplete theory [8]. Thus, a lot of effort from phenomenologists and theorists has been invested in models beyond the SM (now interpreted as a low-energy effective theory), all of which call for extending the particle content of the SM and sometimes, of the gauge symmetry of the model.

Extension of the particle content includes, in its simplest realization, extending the Higgs-boson content. One of the simplest, and most widely studied extension of the SM Higgs sector is the two-Higgs-doublet model (2HDM), where a second scalar Higgs doublet is added, with the same quantum numbers as the existing one [9,10]. There are several versions of the model, depending on the choice of Yukawa couplings of the two doublets. One of these 2HDM is adopted by supersymmetry, where up- and down-type quarks cannot acquire masses by coupling to the same Higgs doublet, see for example [11].

With the addition of the new doublet, the model could provide a new source of charge-parity (*CP*) violation [10,12–14] which is fundamental to explaining matter-antimatter asymmetry of the Universe [15,16].

A significant difference between the *CP*-conserving (*CPC*) and the *CP*-violating (*CPV*) 2HDMs is that, in a

*mariana.frank@concordia.ca
†ericgyabeng2012@gmail.com
‡mtoharia@dawsoncollege.qc.ca

CPC 2HDM, one of the three scalar physical states, identified as the *CP*-odd Higgs boson remains decoupled to the other neutral scalars, whereas in the latter all the three neutral Higgs states mix. One of these states is identified with the 125 GeV Higgs boson, and all three scalar states interact with the gauge bosons. Many detailed studies of *CPC* 2HDMs have been presented, for example in [10,17,18], and other works such as [19–22] have looked at *CPV* 2HDMs using *CP*-odd weak-basis invariants. Also, recent studies of charged Higgs bosons phenomenology in the context of the *CPV* 2HDMs have been presented in [23–27] and a *CPV* 2HDM analysis of viable parameter space regions which pass experimental constraints has been given in [28–32].

The 2HDM Yukawa Lagrangian entails additional features with respect to the SM Lagrangian, which are strongly constrained by experimental data. The main difference is that, in the most general 2HDM Yukawa Lagrangian, flavor changing neutral currents (FCNC) arise at the tree-level [33,34], and these are strongly constrained by experimental data. One can eliminate these dangerous FCNCs by imposing a Z_2 symmetry on the scalar potential and assigning Z_2 charges to the fermions. Various versions of 2HDMs were studied, which can be classified into four different classes based on which type of fermions couple to a specific doublet. These classes are usually grouped as type I, type II, X, and Y [10,35–37].[1]

In this paper we perform a detailed study of the *CPV* 2HDMs with type-II Yukawa couplings. In this model, the couplings of the down-type quarks and charged leptons are proportional to $\tan\beta$, the ratio of the two neutral Higgs bosons vacuum expectation values (VEVs), while the top-quark couplings are proportional to $\cot\beta$, and thus the model is significantly constrained by flavor physics and direct searches of extra Higgs bosons.

Due to its connection with tree-level MSSM, the type-II 2HDM is a popular extension of the Higgs sector [9,38]. While at tree level, the MSSM Higgs sector is strictly *CP*-conserving, it has been shown that under certain circumstances, *CP*-violating effective Higgs sectors could arise via loop corrections [13,39–43]. *CPV* 2HDMs effects in the Higgs sector have been studied extensively in the MSSM limit of the 2HDM in, for example, [44–48].

Here we analyse the consistency of the type-II *CPV* 2HDM with Higgs data, electroweak precision and perturbativity and unitarity constraints, as well as *CPV* in electric dipole moments. Our aim is to investigate in detail the allowed parameter space in the light of the most recent LHC results, in particular the constraints imposed by LHC-Higgs data. In order to study the impact of *CP* violation on the Higgs bosons and their respective decay channels, we consider the *CPV* 2HDM potential parameters [32] in the approximate Z_2 case [49]. We study the various real and reduced couplings in a basis containing the physical states with *CP* violation turned on by fixing the real and imaginary couplings in the scalar potential. The size of these couplings is constrained by perturbativity, unitarity, as well as by electroweak precision parameters, and the imaginary part of these couplings will be further constrained by electric dipole moment (EDM) measurements.

As we increase the amount of *CPV* by turning on the phases in the Higgs potential, we show that constraints from LHC Higgs data still allow some regions of parameter space slightly away from the alignment limit (the region where the SM Higgs boson decouples from the rest of the scalar states). In those viable regions, the masses of the heavy neutral Higgs bosons are tightly constrained by the theoretical and experimental bounds. These constraints prove to be very stringent also in regards to the rest of parameters such as $\tan\beta$, or the mixing angle of the Higgs sector α. Production and decay rates of the heavy neutral Higgs bosons, constrained from these considerations, at the LHC are presented and *CPV* specific signals are highlighted.

Our paper is organized as follows. In Sec. II we present the type-II Two Higgs-doublet model with *CP* violation, concentrating on the parameters in the scalar potential and their effects on the neutral Higgs states. In Sec. III we explore the bounds on the parameters in the context of both theoretical and experimental constraints, from perturbativity and unitarity of the potential, the Higgs data, B-decays, as well as the oblique parameters and the EDMs. In Sec. IV we present the main results, showing the restrictions on the parameter space on the charged and neutral Higgs masses, and in Sec. V we analyze their production cross sections and plot their decay patterns. We summarize and conclude in Sec. VI.

II. TWO-HIGGS-DOUBLET MODEL WITH *CP* VIOLATION

In this section we review the 2HDM considered in this study. We first introduce the most general two-Higgs-doublet scalar potential which breaks $SU(2)_L \times U(1)$ to $U(1)_{\rm EM}$,

$$\begin{aligned} V(\Phi_d,\Phi_u) = &-\frac{1}{2}[m_{11}^2(\Phi_d^\dagger\Phi_d) + (m_{12}^2(\Phi_d^\dagger\Phi_u) + \text{H.c.}) + m_{22}^2(\Phi_u^\dagger\Phi_u)] \\ &+ \frac{\lambda_1}{2}(\Phi_d^\dagger\Phi_d)^2 + \frac{\lambda_2}{2}(\Phi_u^\dagger\Phi_u)^2 + \lambda_3(\Phi_d^\dagger\Phi_d)(\Phi_u^\dagger\Phi_u) + \lambda_4(\Phi_d^\dagger\Phi_u)(\Phi_u^\dagger\Phi_d) \\ &+ \frac{1}{2}[\lambda_5(\Phi_d^\dagger\Phi_u)^2 + \lambda_6(\Phi_d^\dagger\Phi_u)(\Phi_d^\dagger\Phi_d) + \lambda_7(\Phi_d^\dagger\Phi_u)(\Phi_u^\dagger\Phi_u) + \text{H.c.}]. \end{aligned} \tag{2.1}$$

[1]Type-X and type-Y 2HDMs are often known as lepton-specific and flipped 2HDMs, respectively.

where m_{11}, m_{22} and λ_1, λ_2, λ_3, λ_4 are real parameters, while m_{12}^2, λ_6, and λ_7 are complex, and where the Higgs doublets are parametrized as

$$\Phi_d = \begin{pmatrix} \Phi_d^+ \\ \Phi_d^0 \end{pmatrix}, \qquad \Phi_u = \begin{pmatrix} \Phi_u^+ \\ \Phi_u^0 \end{pmatrix}. \tag{2.2}$$

To avoid tree-level flavor changing neutral currents, one imposes a Z_2 symmetry with Higgs bosons obeying the transformation properties,

$$\Phi_d \to -\Phi_d \qquad \Phi_u \to \Phi_u. \tag{2.3}$$

Equation (2.3) implies $\lambda_6 = \lambda_7 = 0$,[2] while we allow a nonzero m_{12} to break softly the Z_2 symmetry of Eq. (2.1).

After electroweak symmetry breaking, the Higgs doublets can be written in terms of the physical states as

$$\Phi_d = \begin{pmatrix} -\sin\beta H^+ \\ \frac{1}{\sqrt{2}}(v\,\cos\beta + h_1^0 - i\,\sin\beta A^0) \end{pmatrix}, \qquad \Phi_u = e^{i\xi}\begin{pmatrix} \cos\beta H^+ \\ \frac{1}{\sqrt{2}}(v\,\sin\beta + h_2^0 + i\,\cos\beta A^0) \end{pmatrix}, \tag{2.4}$$

where $\tan\beta = v_u/v_d$, $v = \sqrt{|v_u|^2 + |v_d|^2} = 246$ GeV and H^+ is the physical charged Higgs boson with mass M_{H^+}. In the neutral scalar sector, there is mixing of the three states, h_1^0, h_2^0 and A_0 due to two independent angles and phases from the imaginary parts of m_{12} and λ_5. The mixing among the three neutral scalars can be parametrized by an orthogonal matrix $\mathcal{R}$ [32],

$$\mathcal{R} = \begin{pmatrix} -\sin\alpha\cos\alpha_b & \cos\alpha\cos\alpha_b & \sin\alpha_b \\ \sin\alpha\sin\alpha_b\sin\alpha_c - \cos\alpha\cos\alpha_c & -\sin\alpha\cos\alpha_c - \cos\alpha\sin\alpha_b\sin\alpha_c & \cos\alpha_b\sin\alpha_c \\ \sin\alpha\sin\alpha_b\cos\alpha_c + \cos\alpha\sin\alpha_c & \sin\alpha\sin\alpha_c - \cos\alpha\sin\alpha_b\cos\alpha_c & \cos\alpha_b\cos\alpha_c \end{pmatrix}, \tag{2.5}$$

with the convention

$$-\frac{\pi}{2} < \alpha_b \le \frac{\pi}{2} \qquad -\pi/2 \le \alpha_c \le \frac{\pi}{2}. \tag{2.6}$$

This form of parametrization is transparent; α mixes the lightest Higgs with the heavier Higgs (as in the CP-conserving case), α_b mixes the lightest Higgs with the CP-odd component, while α_c mixes the heavier Higgs with the CP-odd component. The physical mass eigenstates are then defined as $(h, H_2, H_3)^T = \mathcal{R}(h_1^0, h_2^0, A^0)^T$, with h assumed to the SM-like boson with $M_h = 125$ GeV. This diagonalization procedure yields seven linearly-independent equations that link the physical parameters to the parameters in the scalar potential (see for example [30,32]).

$$\lambda_1 = \frac{M_h^2\sin^2\alpha\cos^2\alpha_b + M_{H_2}^2\mathcal{R}_{21}^2 + M_{H_3}^2\mathcal{R}_{31}^2}{v^2\cos\beta^2} - \nu\tan^2\beta, \tag{2.7}$$

$$\lambda_2 = \frac{M_h^2\cos^2\alpha\cos^2\alpha_b + M_{H_2}^2\mathcal{R}_{22}^2 + M_{H_3}^2\mathcal{R}_{32}^2}{v^2\sin\beta^2} - \nu\cot^2\beta, \tag{2.8}$$

$$\lambda_3 = \nu - \frac{M_h^2\sin\alpha\cos\alpha\cos^2\alpha_b - M_{H_2}^2\mathcal{R}_{21}\mathcal{R}_{22} - M_{H_3}^2\mathcal{R}_{31}\mathcal{R}_{32}}{v^2\sin\beta\cos\beta} - \lambda_4 - \Re\lambda_5, \tag{2.9}$$

$$\lambda_4 = 2\nu - \Re\lambda_5 - \frac{2M_{H^+}^2}{v^2}, \tag{2.10}$$

$$\Re\lambda_5 = \nu - \frac{M_h^2\sin^2\alpha_b + \cos^2\alpha_b(M_{H_2}^2\sin^2\alpha_c + M_{H_3}^2\cos^2\alpha_c)}{v^2}, \tag{2.11}$$

$$\Im\lambda_5 = \frac{2\cos\alpha_b[(M_{H_2}^2 - M_{H_3}^2)\cos\alpha\sin\alpha_c\cos\alpha_c + (M_h^2 - M_{H_2}^2\sin^2\alpha_c - M_{H_3}^2\cos^2\alpha_c)\sin\alpha\sin\alpha_b]}{v^2\sin\beta}, \tag{2.12}$$

[2]This avoids hard breaking of Z_2 symmetry, while soft breaking is still allowed.

$$\tan\beta = \frac{(M_{H_2}^2 - M_{H_3}^2)\cos\alpha_c \sin\alpha_c + (M_h^2 - M_{H_2}^2\sin^2\alpha_c - M_{H_3}^2\cos^2\alpha_c)\tan\alpha\,\sin\alpha_b}{(M_{H_2}^2 - M_{H_3}^2)\tan\alpha\,\cos\alpha_c\,\sin\alpha_c - (M_h^2 - M_{H_2}^2\sin^2\alpha_c - M_{H_3}^2\cos^2\alpha_c)\sin\alpha_b}, \tag{2.13}$$

where $\nu = \Re(m_{12})^2/(v^2\sin 2\beta)$. Note that using Eq. (2.13) in Eq. (2.12) we obtain a much simpler expression for the quartic $\Im\lambda_5$ i.e.,

$$\Im\lambda_5 = \frac{1}{v^2}(M_{H_2}^2\sin^2\alpha_c + M_{H_3}^2\cos^2\alpha_c - M_h^2)\frac{\sin(2\alpha_b)}{\cos(\alpha+\beta)} \quad \text{for } (\alpha_b \neq 0). \tag{2.14}$$

In the CP-conserving version of the 2HDM, $\alpha_b = \alpha_c = 0$, $\mathcal{R}$ is block diagonal, and h and H_2 have no pseudoscalar component.

A. *CP* violation and mixing in the neutral Higgs sector

CP violation can occur in the 2HDM in the scalar sector, and the effects can be considerable. Setting $\lambda_6 = \lambda_7 = 0$ terms, to avoid hard breaking of Z_2 symmetry, we allow it to be only softly broken by the m_{12}^2 term, and using the tadpole equations (obtained by minimizing the Higgs potential Eq. (2.1), we are left with eight independent physical parameters:

(i) Three scalar masses, M_h, M_{H_2}, and $M_{H^\pm}$;
(ii) Three mixing angle α, α_b, α_c in the neutral scalar sector (one from the CP-conserving sector, two from allowing CP violation);
(iii) $\tan\beta = v_u/v_d$, the ratio of VEVs;
(iv) $\Re(m_{12}^2)$, or $\nu \equiv \Re(m_{12})^2/(v^2\sin 2\beta)$.

Here $M_{H_{2,3}}$ are two of the neutral Higgs masses, $M_{H^\pm}$ is the charged Higgs mass, the neutral-sector input mixing angles are α, α_b, α_c, and $\Re(m_{12}^2)$ is the real part of the soft Z_2 breaking parameter.

We fix $M_h = 125$ GeV. As well the third neutral scalar mass M_{H_3} is calculated from the two other ones using the matrix elements of $\mathcal{R}$ [50]

$$M_{H_3}^2 = \frac{M_h^2\mathcal{R}_{13}(\mathcal{R}_{12}\tan\beta - \mathcal{R}_{11}) + M_{H_2}^2\mathcal{R}_{23}(\mathcal{R}_{22}\tan\beta - \mathcal{R}_{21})}{\mathcal{R}_{33}(\mathcal{R}_{31} - \mathcal{R}_{32}\tan\beta)}, \tag{2.15}$$

which reduces the number of independent parameters to seven. In this model, H_3 is, in the limit of no CPV, the CP-odd Higgs, while in the same limit H_2 is the heavy CP-even Higgs. We require the lightest Higgs properties to be consistent with those of the SM-like boson observed at the LHC, and in particular, set its mass to $M_h = 125.35 \pm 0.15$ GeV [51]. We proceed by listing the restrictions imposed on the parameter space of the model. The imaginary part of λ_5, which is a source of CP violation is given in Eq. (2.12).

We concentrate on 2HDMs with a Z_2 symmetry in the Yukawa sector and where Φ_d and Φ_u give mass to only up or down-type fermions, respectively. This corresponds to a CPV version of type-II 2HDMs, leading to suppressed tree-level flavor changing processes mediated by the neutral Higgs scalars. In general, the imposed Z_2 symmetry in the Yukawa sector is not preserved by renormalization, as terms from the Higgs potential will induce couplings of Φ_d, Φ_u to both up- and down-type quarks. However, this does not reintroduce any tree-level flavor changing effects because the induced Yukawa matrices are still proportional to the corresponding fermion-mass matrices. Neglecting mixing from the CKM matrix, the Yukawa Lagrangian is

$$\mathcal{L}_Y = -\left(\frac{\cos\alpha}{\sin\beta}\frac{m_u}{v}\right)\bar{Q}_L(i\tau_2)\Phi_u^* u_R + \left(\frac{\sin\alpha}{\cos\beta}\frac{m_d}{v}\right)\bar{Q}_L\Phi_d d_R + \left(\frac{\sin\alpha}{\cos\beta}\frac{m_\ell}{v}\right)\bar{L}_L\Phi_d e_R + \text{H.c.} \tag{2.16}$$

where $Q_L^T = (u_L, d_L)$, $L_L^T = (\nu_l, \ell_L)$, u, d, and ℓ stand for up- and down-type quarks and leptons, respectively. The couplings between neutral Higgs bosons and the fermions and gauge bosons are

$$\mathcal{L}_{NC} = \sum_{i=1}^{3}\left[-m_f(c_{H_iff}\bar{f}f + \tilde{c}_{H_iff}\bar{f}i\gamma_5 f)\frac{H_i}{v} + (2a_{H_i}m_W^2 W_\mu W^\mu + a_{H_i}m_Z^2 Z_\mu Z^\mu)\frac{H_i}{v}\right]. \tag{2.17}$$

where $H_i = h, H_2, H_3$ and $c_{H_iff}, \tilde{c}_{H_iff} \neq 0$ or $a_{H_i}, \tilde{c}_{H_iff} \neq 0$ indicates CP violation, that is, the mass eigenstate H_i couples to both CP-even and CP-odd operators. The coefficients c_{H_iff}, $\tilde{c}_{H_iff}$ and a_{H_i} are obtained using the

TABLE I. Fermion and gauge-boson couplings to Higgs mass eigenstates.

c_{H_itt}	$c_{H_ibb} = c_{H_i\ell\ell}$	$\tilde{c}_{H_itt}$	$\tilde{c}_{H_ibb} = \tilde{c}_{H_i\ell\ell}$	a_{H_i}
$\mathcal{R}_{i2}/\sin\beta$	$\mathcal{R}_{i1}/\cos\beta$	$-\mathcal{R}_{i3}\cot\beta$	$-\mathcal{R}_{i3}\tan\beta$	$\mathcal{R}_{i2}\sin\beta + \mathcal{R}_{i1}\cos\beta$

matrix $\mathcal{R}$ defined above in terms of α, α_b, α_c, and $\tan\beta$ and are given in Table I.

Thus we can express the couplings presented in Table I in terms of the mixing angles in the scalar sector of the *CPV* 2HDM, α (*CPC*), α_b, and α_c (*CPV*). They represent the 12, 13, and 23 angles from the 3×3 orthogonal diagonalization matrix $\mathcal{R}$ given in Eq. (2.5). For the SM-like Higgs boson, the mixing elements are

$$\mathcal{R}_{11} = -\sin\alpha\cos\alpha_b, \quad \mathcal{R}_{12} = \cos\alpha\cos\alpha_b, \quad \mathcal{R}_{13} = \sin\alpha_b. \tag{2.18}$$

For example, the normalized coupling of top quarks to the SM-like Higgs has the simple expression [52] (in terms of α, β and α_b),[3]

$$|C_{htt}|^2 = \left(\frac{\mathcal{R}_{12}}{\sin\beta}\right)^2 + \left(\frac{\mathcal{R}_{13}}{\tan\beta}\right)^2 = \left(\frac{\cos\alpha\cos\alpha_b}{\sin\beta}\right)^2 + \left(\frac{\sin\alpha_b}{\tan\beta}\right)^2. \tag{2.19}$$

When the Higgs boson mixes with both the *CP*-even and *CP*-odd states, the Higgs coupling to vector bosons V is $a_h \frac{gm_V^2}{M_W} g^{\mu\nu}$, [53], where as above a_h measures the departure from the SM, $a_h = 1$ for a pure *CP*-even state with SM-like couplings and $a_{H_i} = 0$ for a pure *CP*-odd state.

The effects of *CP* mixing will appear also at the loop level, especially in the $gg \to h$ and $h \to \gamma\gamma$ rates. At leading order, the Higgs production rates normalized to the SM expectations can be written as [53,54]

$$\frac{\Gamma(h\to\gamma\gamma)}{\Gamma^{\rm SM}(h\to\gamma\gamma)} \simeq \frac{|\frac{1}{4}a_h A_1^+[m_W] + (\frac{2}{3})^2\Re(C_{htt}) + (\frac{1}{3})^2 A_{1/2}^S[m_b]\Re(C_{hbb})|^2 + |(\frac{2}{3})^2\frac{3}{2}\Im(C_{htt}) + (\frac{1}{3})^2 A_{1/2}^P[m_b]\Im(C_{hbb})|^2}{|\frac{1}{4}A_1^+[m_W] + (\frac{2}{3})^2|^2}$$
$$\frac{\sigma(gg\to h)}{\sigma^{\rm SM}(gg\to h)} = \frac{\Gamma(h\to gg)}{\Gamma^{\rm SM}(h\to gg)} \simeq |\Re(C_{htt}) + A_{1/2}^S[m_b]\Re(C_{hbb})|^2 + \left|\frac{3}{2}\Im(C_{htt}) + A_{1/2}^P[m_b]\Im(C_{hbb})\right|^2, \tag{2.20}$$

with the loop form factors given by [17] $A_1^+[m_W] \simeq -8.32$, $A_{1/2}^S[m_b] \simeq -0.063 + 0.090i$ and $A_{1/2}^P[m_b] \simeq -0.072 + 0.090i$ for $M_h = 125$ GeV.

III. CONSTRAINTS

The *CP*-violating 2HDM is constrained from various theoretical observations and from measurements at collider and noncollider experiments. We first discuss constraints on model parameters from theoretical considerations, then those from the Higgs data, from *B*-physics measurements, from precision data (the *S*, *T*, *U* oblique parameters) and from measurements of EDMs. We restrict ourselves to a brief discussion, and refer to explicit expressions that have appeared before.

A. Perturbativity, vacuum stability, and unitarity

Constraining the theory to be perturbative imposes constraints on all the couplings in the scalar potential

$$|\lambda_i| \lesssim 8\pi. \tag{3.1}$$

In addition, vacuum stability requires the scalar potential, Eq. (2.1), to be positive for large values of Φ_d, Φ_u,

$$\lambda_1 > 0, \quad \lambda_2 > 0, \quad \lambda_3 + \sqrt{\lambda_1\lambda_2} > 0, \quad \lambda_3 + \lambda_4 - |\lambda_5| + \sqrt{\lambda_1\lambda_2} > 0. \tag{3.2}$$

Both unitarity and perturbativity requirements. lead to the constraints [10,55],

$$\left|\frac{1}{2}(\lambda_1+\lambda_2 \pm \sqrt{(\lambda_1-\lambda_2)^2 + 4|\lambda_5|^2})\right| < 8\pi,$$
$$\left|\frac{1}{2}(\lambda_1+\lambda_2 \pm \sqrt{(\lambda_1-\lambda_2)^2 + 4\lambda_4^2})\right| < 8\pi,$$
$$\left|\frac{3(\lambda_1+\lambda_2) \pm \sqrt{9(\lambda_1-\lambda_2)^2 + 4(2\lambda_3+\lambda_4)^2)}}{2}\right| < 8\pi,$$
$$|\lambda_3 \pm \lambda_4| < 8\pi, \quad |\lambda_3 \pm |\lambda_5|| < 8\pi,$$
$$|\lambda_3 + 2\lambda_4 \pm 3|\lambda_5|| < 8\pi. \tag{3.3}$$

[3]Note that the Yukawa couplings for the neutral Higgs bosons H_i with the up-type quarks in the *CPV* 2HDM are $\frac{R_{i2}}{\sin\beta} - i\frac{R_{i3}}{\tan\beta}$, with the first term from the *CP*-even Higgs coupling, and the second from the *CP*-odd coupling.

As the Eqs. (3.1)–(3.3) only depend on the absolute value of λ_5, they do not constrain the *CPV* phases.

These conditions are very important for the *CP*-violating model, as they provide bounds on the masses of the heavy neutral and charged Higgs. From Eqs. (2.10)–(2.11), requiring $-8\pi \leq \lambda_4, \Re\lambda_5 \leq 8\pi$, we obtain the from-above and from-below bounds for $M^2_{H^\pm}$

$$M_h^2 + \cos^2\alpha_b(\tilde{M}^2) - 8\pi v^2 \leq M^2_{H^\pm} \leq M_h^2 + \cos^2\alpha_b(\tilde{M}^2) + 8\pi v^2, \quad (3.4)$$

where we have introduced the mass combination $\tilde{M}^2 = M^2_{H_2}\sin^2\alpha_c + M^2_{H_3}\cos^2\alpha_c - M^2_h$, which is positive, as long as $M^2_h < M^2_{H_i}$. If we now consider Eq. (2.14) and require $-8\pi \leq \Im\lambda_5 \leq 8\pi$, we obtain an upper bound for $\tilde{M}^2$

$$\tilde{M}^2 \leq 8\pi v^2 \frac{|\cos(\alpha+\beta)|}{|\sin 2\alpha_b|}. \quad (3.5)$$

And since $\tilde{M}^2$ is present in the inequality involving $M^2_{H^\pm}$, we can finally obtain the upper bound

$$M^2_{H^\pm} \leq M^2_h + 4\pi v^2\left(2 + \frac{|\cos(\alpha+\beta)|}{|\tan\alpha_b|}\right) \quad \text{for } (\alpha_b \neq 0). \quad (3.6)$$

Note that this bound comes from requiring perturbativity on the quartic couplings λ_4, $\Re\lambda_5$, and $\Im\lambda_5$ and so is not necessarily the strongest bound. Similar upper bounds can be obtained for both $(M^2_{H_2} + M^2_{H_3})$ and ν. From Eq. (2.11) we obtain

$$8\pi\left(\frac{|\cos(\alpha+\beta)|}{|\sin 2\alpha_b|} - 1\right) + \frac{M_h^2}{v^2} \leq \nu \leq 8\pi\left(\frac{|\cos(\alpha+\beta)|}{|\sin 2\alpha_b|} + 1\right) + \frac{M_h^2}{v^2} \quad \text{for } (\alpha_b \neq 0). \quad (3.7)$$

From Eqs. (2.7)–(2.8), imposing $-8\pi \leq \lambda_1, \lambda_2 \leq 8\pi$, we obtain

$$(\nu - 8\pi)v^2 \leq M^2_{H_2} + M^2_{H_3} - \cos^2\alpha_b(\tilde{M}^2) \leq (\nu + 8\pi)v^2, \quad (3.8)$$

and finally, using the previous bounds on $\tilde{M}^2$ we obtain

$$(M^2_{H_2} + M^2_{H_3}) \leq M^2_h + 8\pi v^2 \times \left(2 + \frac{|\cos(\alpha+\beta)|}{|\sin 2\alpha_b|}(1 + \cos\alpha_b^2)\right) \quad \text{for } (\alpha_b \neq 0). \quad (3.9)$$

B. SM Higgs data

The global data set on the SM Higgs boson includes results from LEP, the Tevatron and the more recent LHC experiments. In order to properly combine the constraints coming from the LHC-Higgs data, we used LILITH [53,56]. LILITH is an open-source library written in PYTHON, which can be used in any PYTHON script as well as in C [57] and C++ [58]/ROOT [59] codes, with a command-line interface. At present, LILITH includes the complete data on Higgs measurements at the Tevatron and LHC Run II at 36 fb^{-1}, and only the Higgs production and diboson decay at 139 fb^{-1}.[4]

The SM-like Higgs signal rates and masses are compared with the signal rate measurements, with the additional requirement that the lightest Higgs has a same mass and production and decay properties as the observed Higgs peak in the channels with high mass resolutions $h \to ZZ^\star \to 4\ell$ and $h \to \gamma\gamma$. The signal strength for the 2HDM versus the SM is defined as

$$\mu_i = \frac{\sigma[(gg \to h) \times \text{BR}(h \to X_i)]_{\text{2HDM}}}{\sigma[(gg \to h) \times \text{BR}(h \to X_i)]_{\text{SM}}} \times \omega_i, \quad (3.10)$$

where ω_i are the experimental weights of the measurement which includes the experimental efficiency.

C. *B* Physics constraints

The charged Higgs bosons in the 2HDM contribute to the decays of B mesons and thus B-physics data set can be used to constrain their masses and couplings. Note that, since the couplings of the charged Higgs bosons are not sensitive to the parameters in the neutral sector, these constraints are independent of the amount of *CP* violation in the model. The most stringent constraints on model parameters emerge from the $B \to X_s\gamma$ [61]

$$\text{BR}(B \to X_s\gamma) \leq (3.32 \pm 0.15) \times 10^{-4}, \quad (3.11)$$

and the most restrictive conditions on charged Higgs masses are for $\tan\beta = 1$, where $M_{H^\pm} \geq 580$ GeV [62].

D. S, T, U parameters

This theoretical constraint comes from the oblique parameters, constrained by the global fit [63–65] to be

[4]Other codes such as HIGGSBOUNDS [48] or HIGGSSIGNALS [60] perform similar data analysis but LILITH uses as primary inputs results where production and decay modes are unfolded from experimental categories, while for example HIGGSSIGNALS code uses signal strengths for individual measurements, taking into account the associated efficiencies. The user inputs in LILITH are given in terms of reduced couplings or signal strengths for one or multiple Higgs states.

$$S = 0.00 \pm 0.07, \qquad T = 0.05 \pm 0.06, \qquad U = 0.03 \pm 0.10. \tag{3.12}$$

The oblique parameters S, T, and U are observables that combine electroweak precision data to quantify deviation from the SM and thus are used in any BSM to ensure that the model is consistent with the data.

An alternative way to evaluate the oblique parameters is to fix $U = 0$, motivated by the fact that U is suppressed by an additional factor M_Z^2/M_H^2 compared S and T, which improves the precision on S and particularly on the T parameter, yielding $S = 0.00 \pm 0.07$, $T = 0.05 \pm 0.06$.

The implication of electroweak precision on the mass spectrum of heavier neutral and on the charged Higgs was thoroughly investigated before [66], in the context of *CPV* 2HDM. It was shown that, except for the T parameter, S and U fall well within the experimental bounds. Thus working in the limit $U = 0$ is more conservative, as it restricts the T parameter more. Allowing $U \neq 0$ indicates a strong correlation between T and U parameters, with values of $T > 1$ corresponding to values of $U > 0.01$. In general, the 2HDM can generically produce values for T that exceed the experimental bounds, limiting much of the parameter space.

However, imposing mass splitings [32]: -80 GeV $\leq M_{H^\pm} - M_{H_2} \leq 100$ GeV, and -600 GeV $\leq M_{H^\pm} - M_{H_3} \leq 100$ GeV, insures that the electroweak precision lie in the allowed ranges.

We shall see that our parameter space surviving all constraints is highly degenerate and thus the electroweak corrections are well within experimental bounds. The S, T, and U parameters finite and in principle, observable. Their expressions in are found it, e.g., [67], so we do not repeat them here.

E. Electric dipole moments

The electron EDM measurement places a very strict constraint on the complex Yukawa couplings in most models. In general, the electric dipole moment of a fermion f corresponds to the imaginary parts of the Wilson coefficient d_f of the effective operator

$$\mathcal{L}_{\text{eff}} = d_f \bar{f}_L \sigma_{\mu\nu} f_R F^{\mu\nu} + \text{H.c.} \tag{3.13}$$

Complete expressions for the one-loop evaluation of the EDMs can be found in [30,68,69]. In addition to one-loop contributions, EDMs can originate from two-loop Barr Zee contributions [70], which are proportional to a single power of the electron Yukawa coupling [71,72]. These contributions are more important for type-X (lepton-specific) 2HDM, and still, even in type-X, agreement with low-energy data for the muon anomalous magnetic moment (and significant EDM contributions) require very light pseudoscalar masses and very large values of $\tan\beta$ [73–78], inconsistent with the parameter space analyzed in this model. It has also been shown that, in unlike in the type-I 2HDM, the electron and mercury EDMs are not able to probe the parameter space when $\tan\beta$ is close to 1, which will be our case, due to the cancellation in Barr-Zee diagrams [79]. We have not considered these contributions here.

A recent electron EDM measurement was performed using the ThO molecule in [80]. The constrained quantity is

$$|d_e^{\text{eff}}| < 1.1 \times 10^{-29}\ e \cdot \text{cm}. \tag{3.14}$$

In 2HDM the *CP* violating phase strongly affects the magnitude of the EDM through the modified couplings of the Higgs bosons. In type-II 2HDM the EDM is also expected to be enhanced by $\tan\beta$ [61]. By investigating *CP* violating effects in extended Higgs sector, the electric dipole moment and its effects on produced particles via protons, photons, or electron and positron collisions have all been studied [81–83]. We impose these constraints and explore their effects further in our numerical explorations.

IV. ALLOWED PARAMETER SPACE

In this section, we describe the methodology employed to explore the parameter space. We first investigated the parameter space region by performing detailed calculations of the reduced couplings associated with *CPV* 2HDM and obtained the different signal strengths associated to the SM Higgs. Using LILITH we explored constraints on the model parameters in the $\cos(\beta - \alpha)$ and $\tan\beta$ plane. Once the SM Higgs bounds were considered in this way, we further employed ScannerS [52], a code that performs parameter scans and checks parameter points in BSM theories with extended scalar sectors. ScannerS incorporates theoretical (perturbative unitarity, vacuum stability, boundedness from below) and experimental constraints (electroweak precision, flavor constraints, Higgs searches and measurements, EDMs) from several different sources in order to determine whether a parameter point is allowed or excluded at approximately 95% C.L.

The constraints on the $\cos(\beta - \alpha)$ and $\tan\beta$ plane due to LHC-Higgs data are presented in Fig. 1 which shows the allowed parameter space for different choices of the α_b angle, a measurement of the amount of *CPV* admixture within the SM-like Higgs. Note that the composition of the SM-like Higgs, and thus the allowed parameter region plotted, is independent of α_c, which affects only the amount of *CPV* admixture in the other neutral Higgs bosons. The top left-handed panel shows the parameter restrictions for the *CP*-conserving case $\alpha_b = 0$, where we see that a significant region of the parameter space survives away from the alignment region [for which $\cos(\beta - \alpha) = 0$]. The interesting particularity of this away-from-alignment region is that the bottom quark Yukawa coupling c_{hbb} is negative while the top Yukawa coupling does not flip sign [84,85].

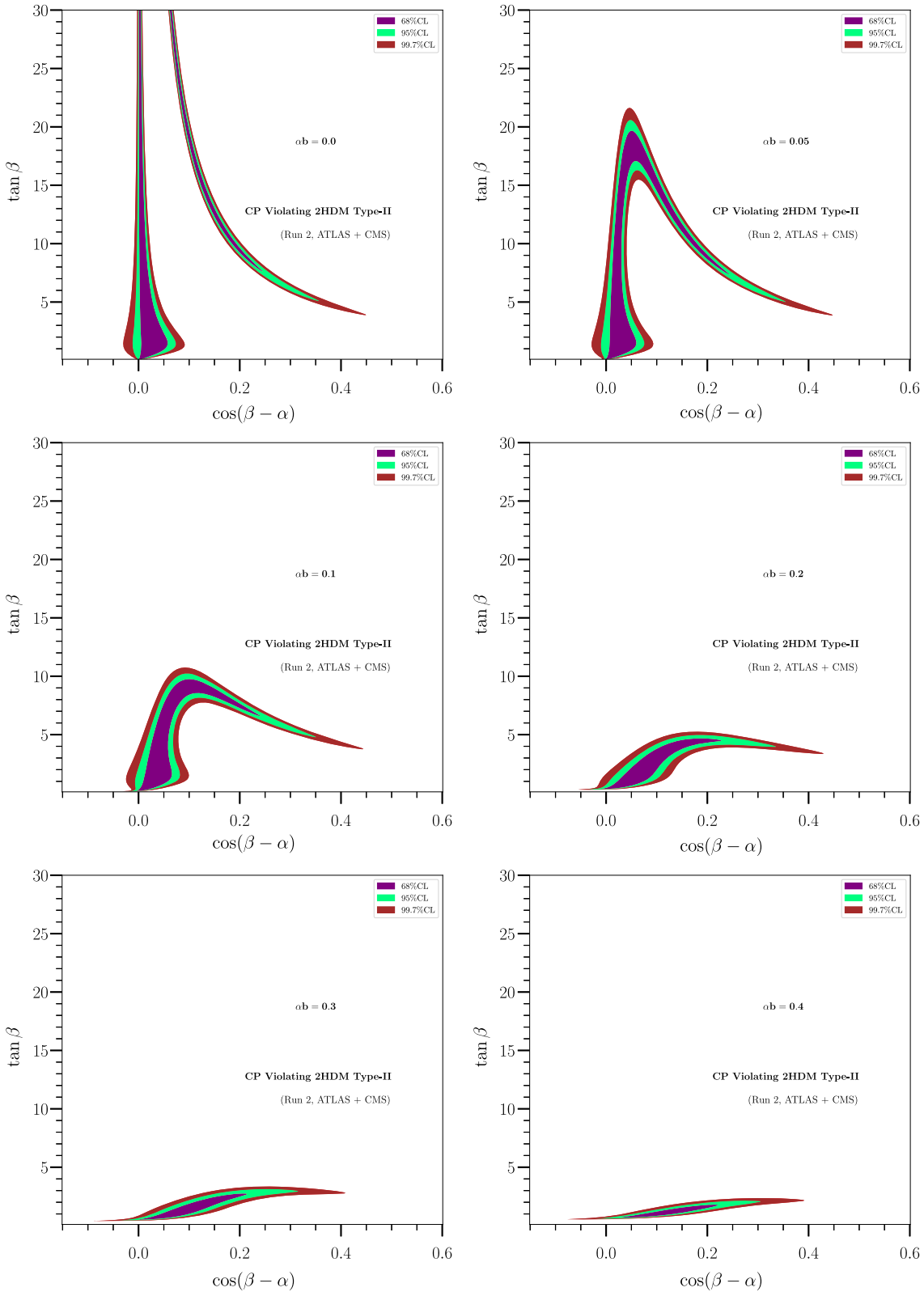

FIG. 1. Allowed parameter space for the 2HDM with *CP* violation from LHC-Higgs data. We show restrictions on the parameter space coming from varying tan β and $\cos(\beta-\alpha)$. Each plot has a fixed value of α_b (measuring the amount of *CP*-violating admixture within the SM-like Higgs boson). Top left: $\alpha_b = 0$ (*CP*-conserving SM-like Higgs), top right: $\alpha_b = 0.05$, middle left: $\alpha_b = 0.1$, middle right: $\alpha_b = 0.2$, bottom left: $\alpha_b = 0.3$, bottom right: $\alpha_b = 0.4$. We included all CMS and ATLAS data at 36 fb^{-1}, as well as data on the Higgs production and diboson decays at 140 fb^{-1} as in the latest LILITH software [56].

Also note that this plot is consistent with more recent phenomenological studies of 2HDM such as [86]. The parameter $\cos(\beta-\alpha)$ determines the c_{hVV} and c_{HVV} couplings and is a measure of deviations from alignment. As usual, $\tan\beta$, the ratio of VEVs, is important in determining the relative strength of the couplings c_{hbb} and c_{htt} (and similarly for $c_{H_{2,3}bb}$ and $c_{H_{2,3}tt}$). Increasing α_b changes significantly the parameter space, in particular, it reduces the allowed values for $\tan\beta$, which can be large at $\alpha_b = 0$, but has a maximum value of about 20 for $\alpha_b = 0.05$ (top right panel), decreasing to about 10 for $\alpha_b = 0.1$ (middle left panel), about 5 for $\alpha_b = 0.2$ (middle right panel), about 3 for $\alpha_b = 0.3$ (bottom left panel) and about 2 for $\alpha_b = 0.4$ (bottom right panel).

In all graphs the regions of the allowed parameter space shrink considerably when increasing α_b (as expected) but noticeably, the region away from alignment survives. This is significant because the away-from-alignment region is a harbinger of nonstandard behavior in the Higgs sector. In the figure, the maroon points correspond to 3σ agreement with the data, green points correspond to 2σ and purple points to 1σ agreement. Increasing α_b leads to slowly shrinking of the parameter regions consistent with experiment, and for $\alpha_b = 0.4$ almost the whole parameter space is excluded, with only a few points near the alignment region surviving. Still, it is interesting to note that, for $\alpha_b = 0.1$, parameter points consistent with the Higgs data at 2σ survive, in both the alignment and away-from-alignment regions.

As mentioned before, the LILITH code, which is self-contained, combines different Higgs signal constraints from published data at 36 fb^{-1}, with the addition of the measurement at 139 fb^{-1} for the process $gg \to h \to ZZ$. The combination of all the most recently published signals has not been fully implemented yet in LILITH. Nevertheless, it is possible to show the evolution of each individual bound and gain an insight on the type of pressure that each Higgs signal puts on the parameter space considered here. We find that the allowed parameter space is most sensitive to three main Higgs signals, namely the $b\bar{b}$, VV, and $\gamma\gamma$ channels. Sensitivity to the rest of Higgs decay channels is less important as their bounds on the parameter space under consideration are always less restrictive than the mentioned signals.

To display the effect of reduced experimental error bars thanks to improved statistics and analysis, we will focus on three individual studies from the ATLAS Collaboration, comparing their older results at 36 fb^{-1} with their most recent bounds with 139 fb^{-1}. In Fig. 2 we chose two examples within the same parameter space as Fig. 1, one for $\alpha_b = 0.1$, the other for $\alpha_b = 0.3$. We show contours for the signal strengths of the Higgs channels $gg \to h \to ZZ$ (red-thick), $Vh \to (h \to b\bar{b})$ (green-light) and $gg \to h \to \gamma\gamma$ (black-thin), using the bounds set by ATLAS, with

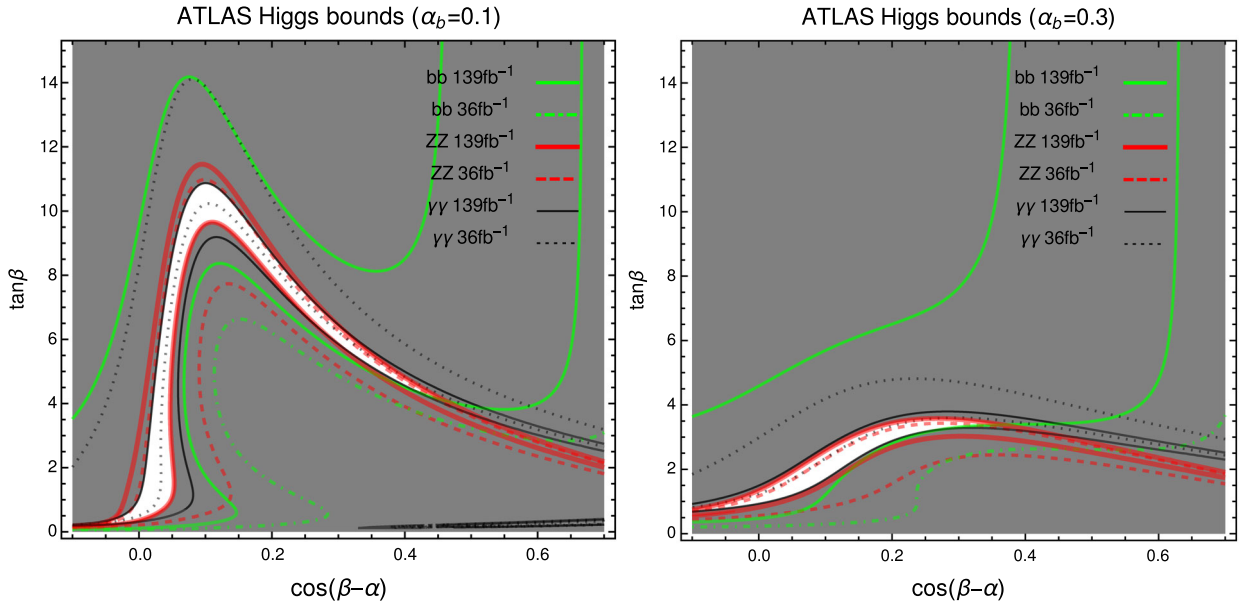

FIG. 2. Contours of the signal strengths for the three Higgs channels $gg \to h \to ZZ$ (red-thick), $Vh \to (h \to b\bar{b})$ (green-light) and $gg \to h \to \gamma\gamma$ (black-thin), using the upper and lower bounds from the ATLAS detector obtained with 36 fb^{-1} (dashed, dot-dashed and dotted respectively) and with 139 fb^{-1} (all solid) of integrated luminosity. The white regions are points in parameter space that individually lie within the $b\bar{b}$, the ZZ and the $\gamma\gamma$ bounds using the 139 fb^{-1} of luminosity from ATLAS. The gray regions represent points that are outside of either of the bounds, i.e., these regions do not represent a combination of bounds. We take $\alpha_b = 0.1$ in the left panel and $\alpha_b = 0.3$ in the right panel. In both cases the individually allowed regions from each of the three Higgs signals is located in between their respective contour curves and clearly shrink when going from 36 fb^{-1} to 139 fb^{-1} of integrated luminosity (although note that the upper bound from $b\bar{b}$ at 36 fb^{-1} does not appear in the plot).

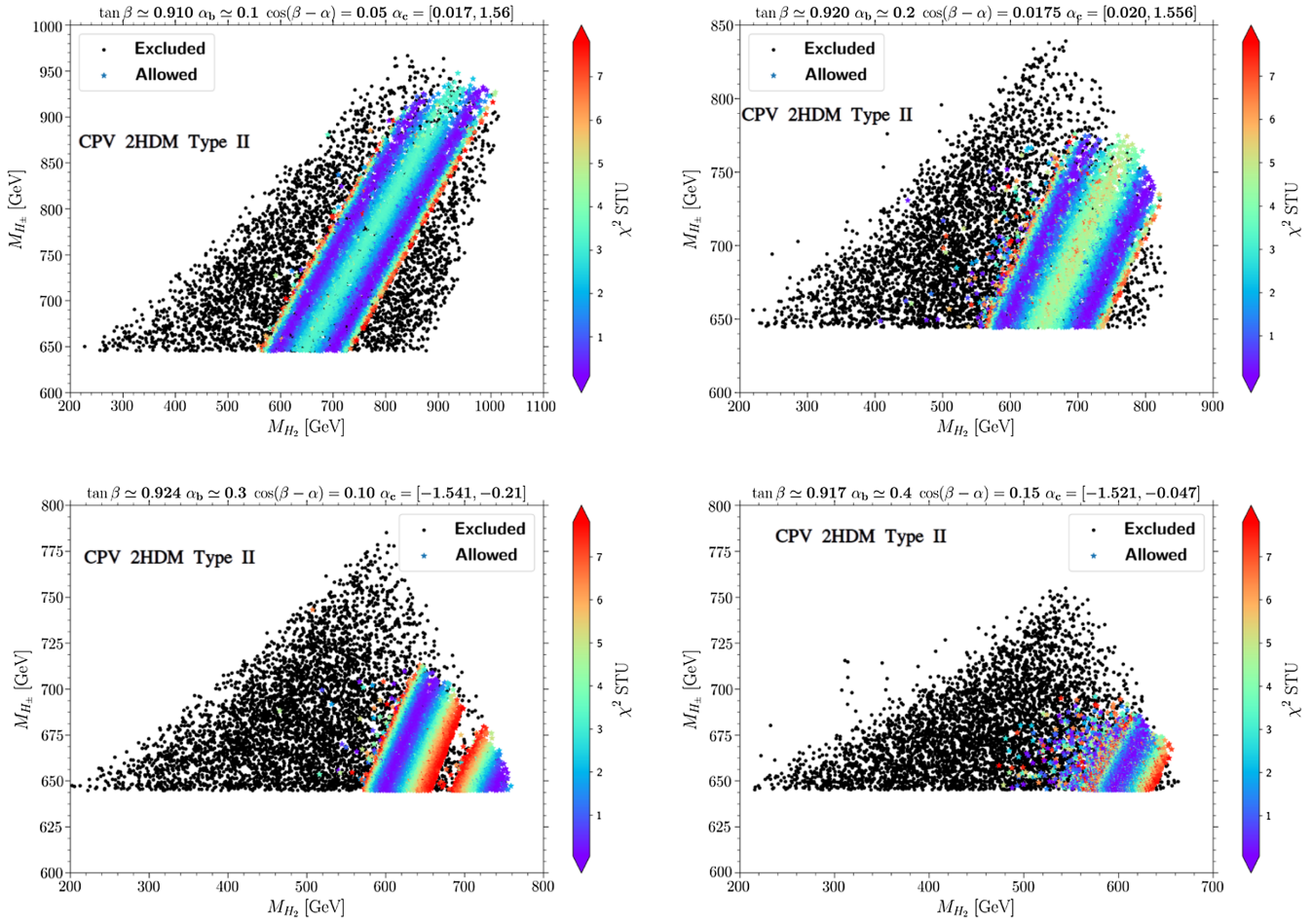

FIG. 3. Restrictions for the *CPV* 2HDM on the parameter space in $M_{H^\pm} - M_{H_2}$ plane from oblique parameters and EDMs. We show plots for different values of $\sin\alpha_b$. Top left: $\alpha_b = 0.1$, top right: $\alpha_b = 0.2$, bottom left: $\alpha_b = 0.3$, bottom right: $\alpha_b = 0.4$. The black dotted region is populated by points that pass all experimental and theoretical bounds, except for precision electroweak tests and EDMs. The rainbow-colored region contains points passing all tests described in Sec. III.

36 fb^{-1} (dashed/dot-dashed/dotted) and with 139 fb^{-1} (solid) of integrated luminosity [87–89]. In both cases, the white regions are points in parameter space that lie individually within the bounds from $b\bar{b}$, ZZ, and $\gamma\gamma$, using the ATLAS data at 139 fb^{-1} of luminosity. Note that these regions do not represent a combination of bounds, but are merely representative of the parameter space that will likely still be allowed once the bounds are properly combined.[5] The improved statistics observed are clearly apparent in the three signal contours with shrinking of the allowed regions as data is improved from 36 fb^{-1} to 139 fb^{-1}. This indicates that while our chosen parameter points are not ruled out, they are under more pressure, and may fit the new data with less C.L.

After delineating the allowed and excluded regions of parameter space using the LHC Higgs data, we proceed to investigate the constraints of the *CP*-violating phases α_b and α_c on the masses of the heavier neutral Higgs bosons H_2 and H_3 and on the mass of the charged Higgs boson $H^\pm$.

In Fig. 3 we show the surviving parameter space in the $M_{H^\pm} - M_{H_2}$ plane, where H_2 is the lightest of the two non-SM like neutral Higgs bosons. In these plots α_b, $\cos(\beta - \alpha)$ and $\tan\beta$ are fixed such that we are within an allowed parameter space point from Fig. 1. In the four plots we fix $\alpha_b = 0.1$ (top left panel), $\alpha_b = 0.2$ (top right panel), $\alpha_b = 0.3$ (bottom left) and $\alpha_b = 0.4$ (bottom right panel). The other *CP*-violating mixing angle α_c is scanned over all possible values but the experimental constraints restrict α_c to lie in the range given in each plot.

The black dots represent the regions allowed by all constraints in Sec. III, except for EDMs and oblique parameters (we use ScannerS). We have chosen a parameter space region allowed by Higgs data (see Fig. 1) and the main bounds on the black-dotted region come from B-physics constraints which are responsible for the

[5]Performing such a combination is beyond the scope of the present paper.

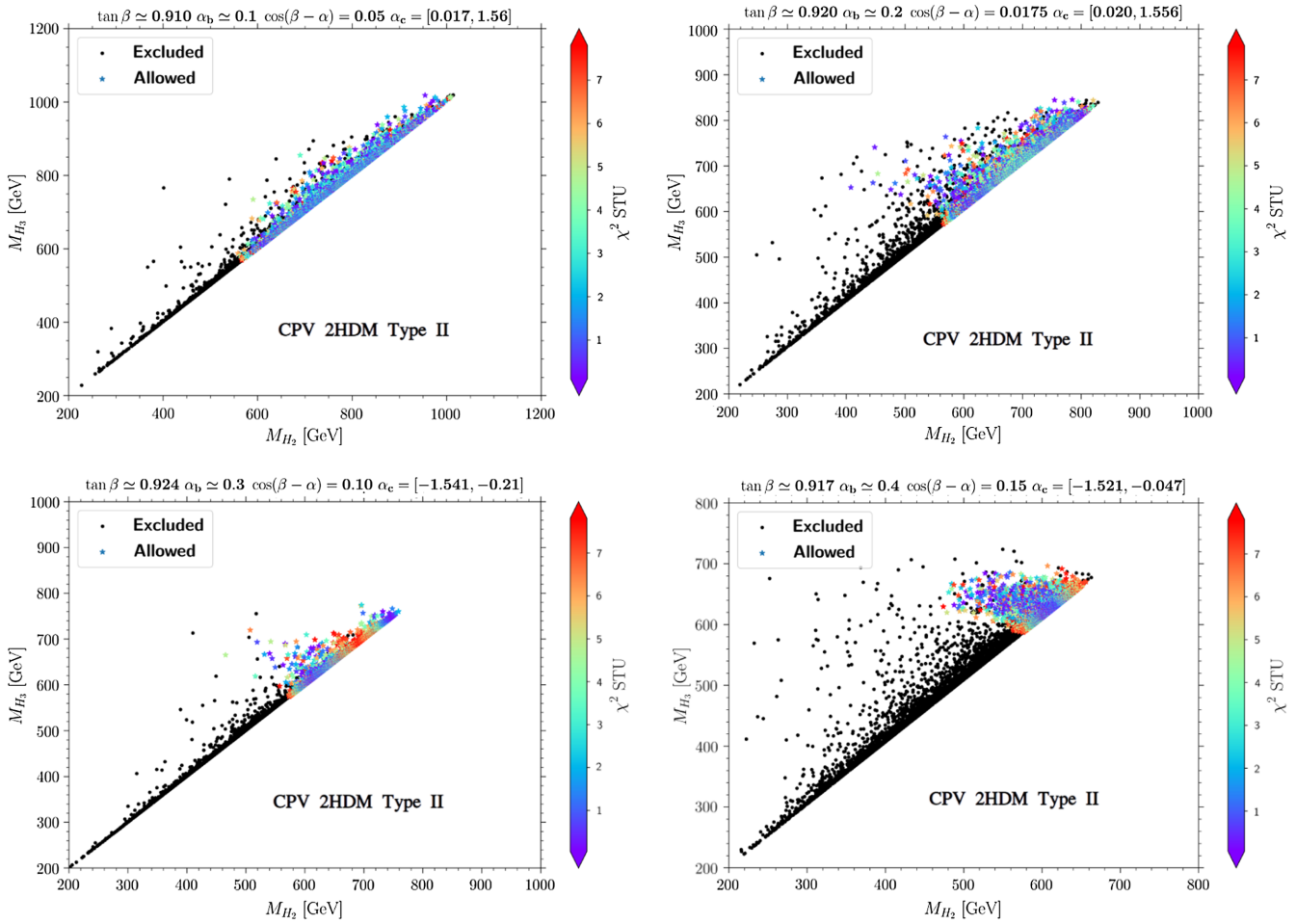

FIG. 4. Restrictions for the 2HDM with *CP* violation on the parameter space for M_{H_3} and M_{H_2} plane from oblique parameters. We show plots for different values of $\sin\alpha_b$. Top left: $\alpha_b = 0.1$, top right: $\alpha_b = 0.2$, bottom left: $\alpha_b = 0.3$, bottom right: $\alpha_b = 0.4$. The black dots are points that pass all experimental and theoretical bounds, except for precision electroweak tests and EDMs. The rainbow-colored dots are points that pass all tests described in Sec. III.

requirement $M_{H^\pm} \geq 650$ GeV. In addition, perturbativity and unitarity requirements which restrict the parameter space to within the diagonal border-lines at the left, right and top of each plot. In particular one can see that direct unitarity and perturbativity constraints involve the coupling λ_4, which depends explicitly on both the charged Higgs mass and the neutral Higgs masses [see Eqs. (2.9) and (2.10)]. Within the *CP*-violating parameters considered here, these unitarity and perturbativity requirements make $M_{H^\pm}$ bound from above, disallowing it to be much larger than M_{H_2} and M_{H_3}, as shown in the discussion in Sec. III A.

Inside the black dotted region, we show as the rainbow-colored region, the physical domain that passes all tests, including electroweak precision measurements constraints from the oblique parameters (*STU*), as in III D, and *CPV* constraints from electric dipole moments, as in III E. The legend at the right shows the deviation from the prescribed *STU* and EDM parameters as measured by χ^2, restricted to be < 7. We find that, within the allowed parameter region of Fig. 1, points that pass *STU* and EDM constraints require an almost fixed value for $\tan\beta$, consistently around $\tan\beta \sim 0.9$ and always smaller than 1.[6] The reason is that a relative mass degeneracy among the heavy scalars is necessary to avoid precision tests bounds, and with nonzero *CP* violation, the masses of the three neutral scalars are all connected via $\tan\beta$ [see Eq. (2.13)]. One can check that for small values of $\cos(\beta-\alpha)$ (i.e., for $\beta \sim \alpha + \pi/2$) a small mass splitting between M_{H_2} and M_{H_3} can only happen when $\tan\beta \sim 1$.

The parameter regions chosen in all four graphs correspond to regions slightly away from alignment in which $\cos(\beta-\alpha) > 0$. In the case of *CP* conservation, and in the decoupling limit, the mass M_h is independent of the other two neutral boson masses (one *CP*-even, one *CP*-odd) which are not restricted. This is not the case for the *CPV* case, and slightly away from the decoupling limit. Here the parameter α_c which determines the *CP* admixture in the

[6]Note that while in MSSM, $\tan\beta$ must be greater than 1, $\tan\beta$ is not restricted in 2HDMs.

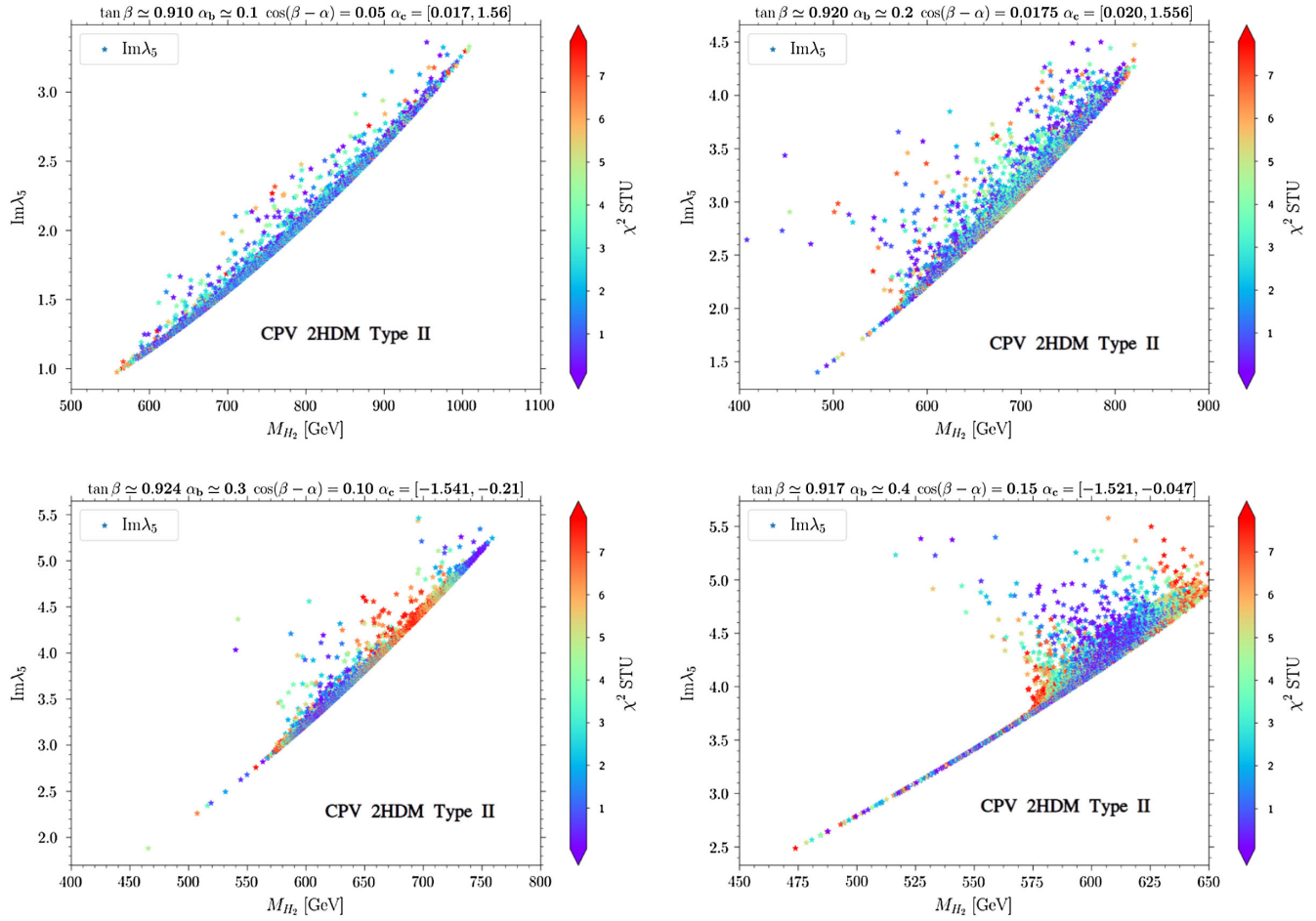

FIG. 5. Constraints on $\Im\lambda_5$, a source of CPV in the Lagrangian of the 2HDM, versus M_{H_2} from oblique parameters. We show plots for different values of α_b. Top left: $\alpha_b = 0.1$, top right: $\alpha_b = 0.2$, bottom left: $\alpha_b = 0.3$, bottom right: $\alpha_b = 0.4$. The rainbow colored dots are points that pass all tests described in Sec. III, including precision tests and EDM bounds.

heavier neutral bosons H_2 and H_3 is varied but only values within a limited range lead to allowed points, the exact interval depending on the value α_b chosen. Increasing α_b enhances the amount of *CPV* admixture in the SM-like Higgs boson resulting in a decrease in the allowed range by EDMs and *STU* constraints in the $M_{H^\pm} - M_{H_2}$ plane. The allowed regions (in rainbow colors) are separated by straight diagonal lines in $M_{H^\pm} - M_{H_2}$, and while the allowed window for M_{H_2} is approximately constant, $M_{H_2} \sim 550 \to 700$–1000 GeV. The range for $M_{H^\pm}$, while being run into the TeV region, is restricted by unitarity and perturbativity requirements, as explained above. $M_{H^\pm}$ shrinks considerably with increasing α_b, from 650–950 GeV for $\alpha_b = 0.1$ in the top left hand panel, to 650–685 GeV for $\alpha_b = 0.4$, in the bottom right hand panel. We also note that regions slightly more separated from alignment survive for larger values of α_b, such as for $\alpha_b = 0.4$, where a small region of parameter space is allowed for $\cos(\beta - \alpha) \simeq 0.15$. In this region, $\Gamma(H_{2,3} \to VV) \neq 0$ and hence, the decay of the heavy neutral Higgs into the electroweak gauge bosons is allowed.

In Fig. 4, we show the allowed parameter space in the M_{H_3} versus M_{H_2} plane from imposing all constraints except the EDMs and the *STU* parameters (black points), and with EDMS and oblique parameters (rainbow-colored points). Here, the mass of the charged Higgs was varied in the allowed ranges from Fig. 3. The relationship between the masses (squared) of the two neutral heavy scalars is linear, and lies in a restricted range. In all cases we find that these two masses must be relatively degenerate in mass in order to satisfy experimental constraints, in particular restrictions from the *STU* parameters. The allowed ranges for both masses shrink with increasing α_b, but note also that for larger values of α_b the degeneracy requirement between the two masses is slightly relaxed.

In the *CPV* 2HDM model, a main source of *CP* violation is encapsulated in $\Im\lambda_5$, given in Eq. (2.12). From [30,90–93], the unitarity bound on $\Im\lambda_5$ should be $\Im\lambda_5 < 4\pi$. The value depends on the *CP*-violating mixing angles α_b, α_c and on the masses M_{H_2} and M_{H_3}. We show in Fig. 5 below, $\Im\lambda_5$ as a function of M_{H_2}. As before the mass of the SM-like Higgs boson h is kept at 125.09 GeV, and

we also take the same input parameters as in Fig. 4. We show here only the rainbow-colored points, that is, points that survive all constraints, including EDMs and *STU* bounds.

V. PRODUCTION AND DECAY OF HEAVY HIGGS BOSONS AT THE LHC

We now proceed to analyze the implications of the restrictions on the parameter space of $M_{H_2}, M_{H_3}, M_{H^\pm}$ on the production and decay rates of the heavy gauge bosons at the LHC. We analyze regions of parameter space that pass all restrictions, as shown in Figs. 3 and 4.

A. Neutral Higgs bosons production

The heavier Higgs bosons are expected to be produced at the LHC dominantly via the gluon fusion process $gg \to H_{2,3}$. Additional production processes include vector boson fusion $pp \to H_{2,3}qq'$, vector boson associated production $pp \to H_{2,3}V$, and top associated production $gg \to H_{2,3}t\bar{t}$.

In this work we employ SusHi [94] to calculate cross sections for gluon fusion to next to leading order (NLO), At one loop, for the gluon fusion process, the ratio of the heavy Higgs boson production cross section in a *CPV* 2HDM to that of a SM-like Higgs is

$$R^i_{gg} = \frac{\sigma(gg \to H_i)}{\sigma(gg \to h)} = \frac{|c_{H_itt}A^H_{1/2}(\tau^i_t) + c_{H_ibb}A^H_{1/2}(\tau^i_b)|^2 + |\tilde{c}_{H_itt}A^A_{1/2}(\tau^i_t) + \tilde{c}_{H_ibb}A^A_{1/2}(\tau^i_b)|^2}{|A^h_{1/2}(\tau_t) + A^h_{1/2}(\tau_b)|^2}, \tag{5.1}$$

where $\tau^i_f = M^2_{H_i}/(4m^2_f), \tau_f = M^2_h/(4m^2_f)$ and $i = 2, 3$, $f = t, b$. The functions $A^H_{1/2}$, $A^A_{1/2}$ are given by

$$A^H_{1/2}(\tau) = 2(\tau + (\tau - 1)f(\tau))\tau^{-2}, \tag{5.2}$$

$$A^A_{1/2}(\tau) = 2f(\tau)\tau^{-1}, \tag{5.3}$$

$$f(\tau) = \begin{cases} \arcsin^2(\sqrt{\tau}), & \tau \le 1 \\ \frac{1}{4}\left[\log\left(\frac{1+\sqrt{1-\tau^{-1}}}{1-\sqrt{1-\tau^{-1}}}\right) - i\pi\right]^2, & \tau > 1 \end{cases}. \tag{5.4}$$

The above expressions are given at LO. In our numerical evaluation, the production cross sections via gluon fusion are calculated at NLO using SusHiv1.6.0 [94] and interfaced with ScannerS [52]. As neutral Higgs bosons in our model have no definite *CP* assignment, *CP*-even and *CP*-odd contributions are summed over [50,93]. In addition, all decay channels including the dominant higher-order effects such as radiative corrections and multibody channels are included as in HDECAY [95,96].

B. Neutral heavy Higgs-boson decay rates

The heavy neutral scalar Higgs bosons decay rates into electroweak gauge bosons are

$$\Gamma(H_i \to VV) = (a_{H_i})^2 \frac{G_F M^3_{H_i}}{16\sqrt{2}\pi}\delta_V\left(1 - \frac{4m^2_V}{M^2_{H_i}}\right)^{1/2}\left[1 - \frac{4m^2_V}{M^2_{H_i}} + \frac{3}{4}\left(\frac{4m^2_V}{M^2_{H_i}}\right)^2\right], \tag{5.5}$$

where $V = W, Z$, $\delta_W = 2$, $\delta_Z = 1$, and $i = 2, 3$. We note that in the alignment limit, $\Gamma(H_{2,3} \to VV) = 0$ when $\sin\alpha_b = \sin\alpha_c = 0$, or away from alignment. These channels open up for nonzero *CP* violation. The decay rates of the neutral Higgs bosons to SM fermions are

$$\Gamma(H_i \to \bar{f}f) = \frac{N_c G_F m^2_f M_{H_i}}{4\sqrt{2}\pi}\left\{(c_{H_iff})^2\left(1 - \frac{4m^2_f}{M^2_{H_i}}\right)^{3/2} + (\tilde{c}_{H_iff})^2\left(1 - \frac{4m^2_f}{M^2_{H_i}}\right)^{1/2}\right\}, \tag{5.6}$$

where $N_c = 3$ for quarks and 1 for charged leptons.

The heavy scalars can also decay to a pair of gluons via a loop of top or bottom quarks, and the rates are

$$\Gamma(H_i \to gg) = \frac{\alpha^2_s G_F M^3_{H_i}}{64\sqrt{2}\pi^3}[|c_{H_itt}A^H_{1/2}(\tau^i_t) + c_{H_ibb}A^H_{1/2}(\tau^i_b)|^2 + |\tilde{c}_{H_itt}A^A_{1/2}(\tau^i_t) + \tilde{c}_{H_ibb}A^A_{1/2}(\tau^i_b)|^2]. \tag{5.7}$$

As the decay rate is a CP-even quantity, in all the above decay rates, the CP-even coefficient $c_{H_i ff}$ and the CP-odd one $\tilde{c}_{H_i ff}$ always contribute incoherently. In addition the heavy neutral scalars, H_2, H_3 can decay into the Z boson and the SM-like Higgs boson h,

$$\Gamma(H_i \to Zh) = \frac{|g_{H_i Zh}|^2}{16\pi M_{H_i}^3}\sqrt{(M_{H_i}^2-(M_h+m_Z)^2)(M_{H_i}^2-(M_h-m_Z)^2)} \times\left[-(2M_{H_i}^2+2M_h^2-m_Z^2)+\frac{1}{M_Z^2}(M_{H_i}^2-M_h^2)^2\right], \tag{5.8}$$

where $g_{H_i Zh} = (e/\sin 2\theta_W)[(-\sin\beta\mathcal{R}_{11}+\cos\beta\mathcal{R}_{12})\mathcal{R}_{i3}+(\sin\beta\mathcal{R}_{i1}-\cos\beta\mathcal{R}_{i2})\mathcal{R}_{13}]$. We have also calculated the decay rate of $H_i \to hh$ from the Higgs self-interactions. The decay rate is [97]

$$\Gamma(H_i \to hh) = \frac{g_{H_i hh}^2}{8\pi M_{H_i}}\sqrt{1-\frac{4M_h^2}{M_{H_i}^2}}, \tag{5.9}$$

where $g_{H_i hh}$ $(i = 2, 3)$ are [98]

$$g_{H_i hh} = \frac{1}{4v\ \sin 2\beta}\{4\cos^2(\beta-\alpha)\cos(\beta+\alpha)|m_{12}|^2-[\cos(3\alpha-\beta)+3\cos(\beta+\alpha)]M_h^2\}\mathcal{R}_{i1} + \frac{\cos(\beta-\alpha)}{2v\ \sin 2\beta}\{(3\ \sin 2\alpha-\sin 2\beta)|m_{12}|^2-\sin 2\alpha(2M_h^2+M_{H_i}^2)\}\mathcal{R}_{i2}. \tag{5.10}$$

To obtain the branching ratios, we include the total width of the heavy Higgs,

$$\Gamma_{\rm tot}(H_i) = \Gamma(H_i \to W^+W^-)+\Gamma(H_i \to ZZ)+\Gamma(H_i \to t\bar{t})+\Gamma(H_i \to b\bar{b}) + \Gamma(H_i \to \tau^+\tau^-)+\Gamma(H_i \to gg)+\Gamma(H_i \to Zh)+\Gamma(H_i \to hh). \tag{5.11}$$

The branching ratios of the various physical scalars in CPV 2HDM were calculated using C2HDM HDECAY [50] through the HDECAY interface [95,96,99]. Predictions for gluon-fusion Higgs production at hadron colliders for the scalars were obtained using tabulated results from SusHi [94] at NLO. We insert the CPV 2HDM model by turning on the CP-violating angles, α_b and α_c. From our parameter space investigations, we find that the maximum CP-violating angle α_b allowed by the Higgs signal strength measurements from the LHC is around $\alpha_b \simeq 0.4$ as shown on the bottom right panel in Fig. 1.

In Figs. 6 and 7, we present the results for the production cross sections times the branching ratios of H_2 and H_3, respectively, for various mixing angles $\cos(\beta-\alpha)$ and CPV angles. For consistency, we maintain the same parameter space analysed in Fig. 3.

In our analysis, the second and third neutral Higgs are close in mass, as a result of the STU constraints, and because of this, the heavy neutral Higgs bosons decay only into SM particles. The mass of the charged Higgs boson is initially randomly scanned although its value is restricted to lie within the allowed range [note that the third neutral Higgs mass is not an independent parameter, but computed from the mass of the lighter neutral Higgs bosons and the various angles as shown in Eq. (2.15)].

We show results for the production and decay of the heavy Higgs slightly away from the alignment limit [in which $\cos(\beta-\alpha) = 0$]. The results shown in Figs. 6 and 7 are such that $\cos(\beta-\alpha) = 0.05$ on the top left, $\cos(\beta-\alpha) = 0.0175$ on the top right, $\cos(\beta-\alpha) = 0.1$ on the bottom left and $\cos(\beta-\alpha) = 0.15$ on the bottom right, and are all in a parameter space region allowed by LHC Higgs data from Fig. 1.

Note that the mass regions in each plot are different. This is because we show, in each panel, the M_{H_2} and M_{H_3} regions and α_c range surviving the constraints for the chosen values of α_b and $\cos(\beta-\alpha)$, consistent with the allowed ones in Fig. 3.

In this regime, the decays into gauge bosons are open, in both the CP-even final states (ZZ and WW) and in the CP-odd final state (Zh). We plot as solid (dotted) lines, the production times branching ratios for H_2 for the minimum and maximum allowed values for α_c from Fig. 3, while keeping the same colour convention for each channel.

In all plots, $H_2 \to t\bar{t}$ is the dominant decay mode, owing to small values of $\tan\beta$. Production and decay rates into

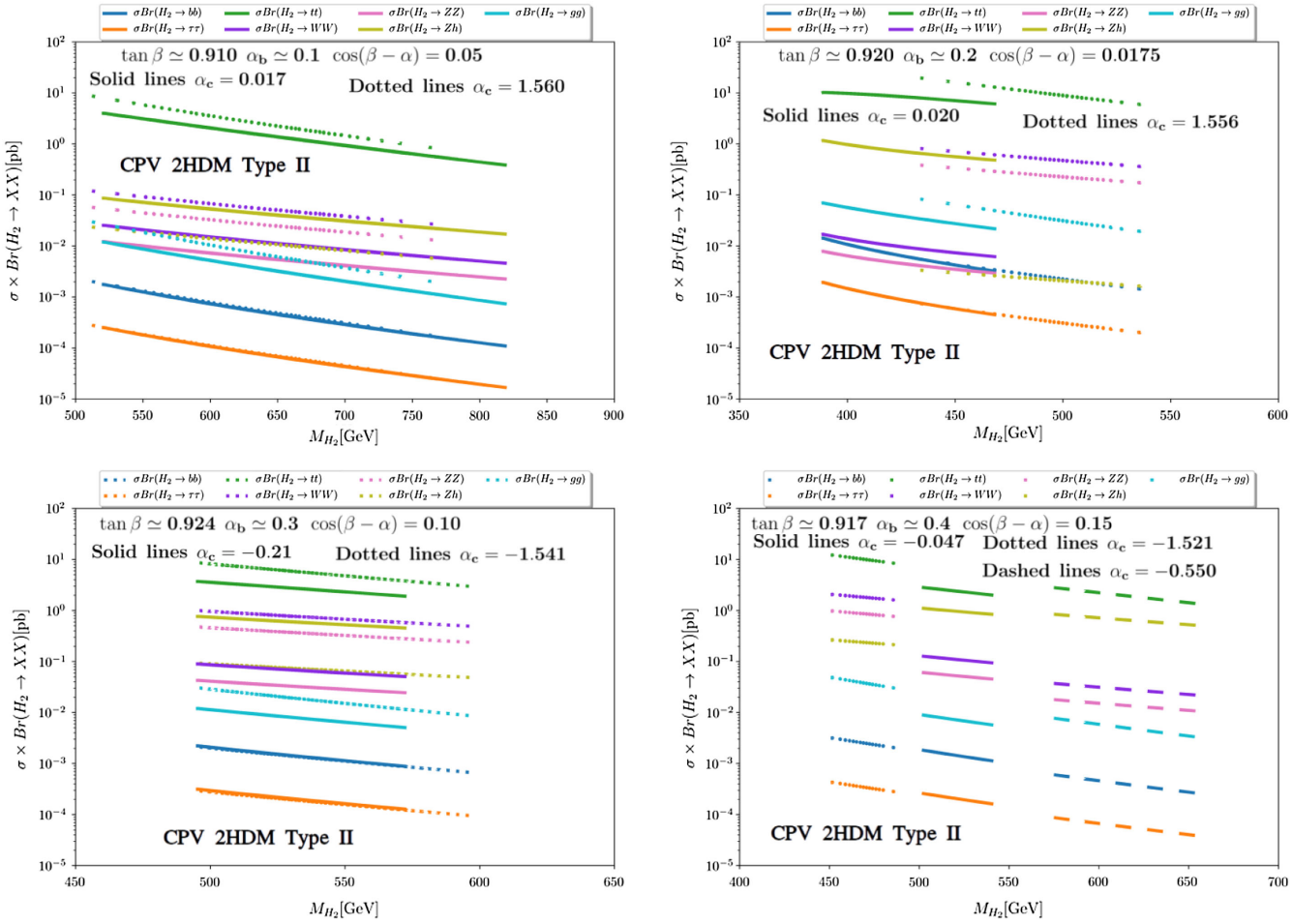

FIG. 6. $\sigma_{gg_{H_2}}$ times branching ratios versus M_{H_2}, in pb, allowed by both STU and EDM constraints for different values of $\sin\alpha_b$. Top left: $\alpha_b = 0.1$, top right: $\alpha_b = 0.2$, bottom left: $\alpha_b = 0.3$, bottom right: $\alpha_b = 0.4$. We plot, in each panel, the M_{H_2} region and α_c range surviving the constraints for the chosen values of α_b and $\cos(\beta-\alpha)$, consistent with the allowed ones in Fig. 3.

gauge bosons can reach $\mathcal{O}(1)$ pb depending on the values of α_b and α_c; similar cross section values can be reached for the CP-odd final state Zh, for different values of the CPV mixing angles. In fact, in all panels we observe how the cross sections between CP-even gauge boson final states and CP-odd final states can flip by changing the value of α_c from its minimum value (solid lines) to its maximum value (dotted lines).

In the two top panels, with $\alpha_b = 0.1$, $\alpha_b = 0.2$, when the value of α_c is close to 0 (solid lines), the decays into Zh represent the main decay channel involving gauge bosons, with the CP-even decay channels into WW and ZZ being between one to two orders of magnitude smaller. This shows that in this limit of small CPV mixing angles, the state H_2 is "mostly" CP-odd. However, as we increase the value of α_c (dotted lines), the decays into CP-even gauge boson channels become larger than into the CP-odd channel Zh, and so the state H_2 can be considered as "mostly" CP-even.

In the lower panels the situation is similar, even though the value of α_b is larger, with $\alpha_b = 0.3$, $\alpha_c = 0.4$. The allowed values of α_c are constrained to be negative, but again when the absolute value of α_c is small (solid lines) the decays in to Zh represent the main decay channel with a gauge boson, so that again, for smaller CPV angles, the state H_2 is "mostly" CP-odd. For a larger absolute value of α_c (dotted lines), the CP-even gauge boson decays become larger than the CP-odd channel Zh, and so the state H_2 is now "mostly" CP-even.

In the top panels and the bottom-left panel, intermediate values of α_c do allow for relatively similar windows for the mass of H_2. However for the case $\alpha_b = 0.4$ only a limited range of mass values for H_2 satisfies the constraints, and this is distinct for every value of α_c. To showcase this effect in the bottom right panel, we also plot the production and decay cross section of H_2 for an intermediate value of α_c, shown by dashed lines. The effect of changing α_c is entirely nonlinear; while the minimum to maximum are slightly shifted from the left (lower masses) to the right (higher masses), the plots for intermediate values of α_c do not fall in between but are shifted further to the right. However, both

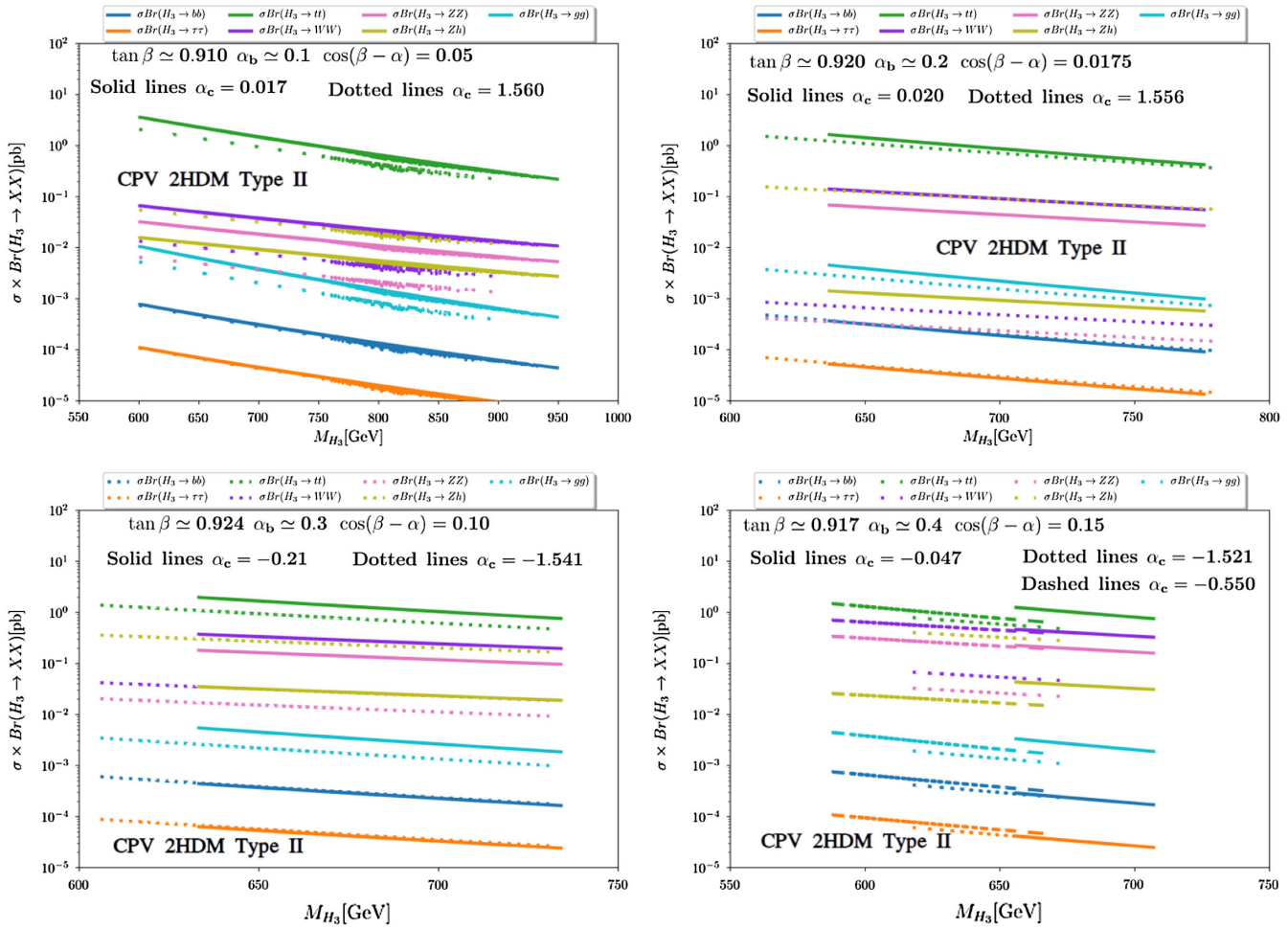

FIG. 7. $\sigma_{gg_{H_3}}$ times branching ratios versus M_{H_3}, in pb, allowed by both STU and EDM constraints, for different values of $\sin\alpha_b$. Top left: $\alpha_b = 0.1$, top right: $\alpha_b = 0.2$, bottom left: $\alpha_b = 0.3$, bottom right: $\alpha_b = 0.4$. We plot, in each panel, the M_{H_3} region and α_c range surviving the constraints for the chosen values of α_b and $\cos(\beta-\alpha)$, consistent with the allowed ones in Fig. 3.

the dashed and solid lines correspond to a "mostly" CP-odd scalar, whereas the "mostly" CP-even scalar corresponds to the dotted line, for the lowest allowed scalar masses.

We expect that plotting all allowed values of α_c will result in uninterrupted lines, each segment corresponding to different α_c's. The slight shifting in masses is noticeable in the other panels, but not as pronounced as for $\alpha_b = 0.4$.

Fig. 7 analyses the same production and decay cross sections for H_3, the heaviest neutral boson. We vary the parameters over the same allowed region as in Fig. 6. The plots show the expected behavior of the heaviest neutral scalar relative to the scalar H_2 with respect to its couplings to gauge bosons. For the parameter values where the scalar H_2 was found to be "mostly" CP-odd (small values of α_c), the scalar H_3 is "mostly" CP-even, meaning its decay cross section into WW or ZZ is dominant over the decay into Zh. And conversely when H_2 is "mostly" CP-even, H_3 then behaves as "mostly" CP-odd.

In all cases the dominant decay channels are $t\bar{t}$, WW, ZZ, and Zh.

The approximate degeneracy of the masses M_{H_3} and M_{H_2} has attracted some interest from phenomenologists. At the LHC, experiments looked for the four lepton final states, resulting from decays into ZZ, often referred to as the golden channel when searching for additional heavy scalar resonances. This is motivated by the fact that the corresponding SM backgrounds are small and controllable. Encouragingly, the four-lepton analyses from ATLAS [100] and CMS [101,102] indicate some enhancement in the event rates in final states with high invariant masses. These analyses were interpreted to be consistent with a broad resonance structure around 700 GeV [103], and most recently, also interpreted as a double peak of degenerate states around 680 GeV in the 2HDM [104]. In their case, the degeneracy is imposed to fit the data, while in our analysis, this scenario is completely consistent and imposed by the experimental and theoretical constraints.

VI. SUMMARY AND CONCLUSION

In the present study, we have explored the allowed parameter space of the type-II two-Higgs-doublet model

with *CP* violation, and the implications for the production and decays of the additional neutral Higgs bosons at the LHC. After implementing the model with approximate Z_2 symmetry, we set some parameters to zero to forbid flavor-changing neutral currents, but still allowing for complex parameters in the potential. We then proceed by restricting the *CP*-violating parameter space using both theoretical considerations and experimental data constraints.

First, we showed that after imposing constraints from the LHC-Higgs data some regions of parameter space very close to alignment as well as relatively away from it survive (the alignment region is such that the heavy Higgs fields decouple from the rest of the spectrum leaving only a single SM-like Higgs within the scalar sector).

Within the allowed regions of parameter space, we imposed theoretical constraints involving vacuum stability, unitarity, and perturbativity, electroweak precision constraints, as well as experimental constraints from *B*-physics and electric dipole moments. We compute the relevant couplings and perform a random scan over two of the 2HDM physical masses, M_{H_2} (the second lightest neutral Higgs) and $M_{H^\pm}$, within parameter regions which satisfy the Higgs data and all other constraints.

The main findings presented in this work, representing new contributions to the study of CVP 2HDM can be listed as follows:

(i) We clearly presented restrictions on the parameter space of the *CPV* 2HDM coming from LHC Higgs data in the plane $\tan\beta$—$\cos(\beta-\alpha)$ (the mixing angle in the neutral Higgs boson sector), for fixed values of α_b, the amount of *CPV* admixture in the lightest (SM-like) Higgs. Our plots, which for $\alpha_b = 0$ coincide with available analyses for the *CP*-conserving 2HDM, also show how the parameter space allowed by Higgs data shrinks with increasing α_b.

(ii) Throughout the *CPV* parameter space explored, $\tan\beta \sim 0.9$ emerges as a solid constraint caused by the necessity of having close to degenerate neutral heavy scalar masses in order to pass precision electroweak tests and EDM's.

(iii) We proved analytically (and confirmed numerically) that in the *CPV* 2HDM the masses of the heavy neutral Higgs, M_{H_2} and M_{H_3}, as well as that of the charged Higgs, $M_{H^\pm}$, are bounded from above. We demonstrated that this is a feature specific to *CPV* only, and is absent in the *CPC* 2HDMs.

(iv) We also show that, for most of the parameter region allowed, and except for small corners of the parameter space (for the largest α_b allowed, and away from alignment), the two heavier neutral Higgs bosons H_2 and H_3 are constrained to be approximately degenerate in mass. This is a condition imposed by *S*, *T* parameters. The latter also affect $\Im\lambda_5$, a measure of *CP* violation in the potential, which is quite large in these scenarios.

(v) While the masses of the charged and neutral Higgs bosons are varied in a large parameter range, they are constrained to lie in a small mass window. We also separate clearly restrictions coming from oblique *S*, *T* parameters and electric dipole moments, from the region which obeys all other experimental and theoretical bounds (such as Higgs data, and *B*-physics constraints).

(vi) While the exact value of the mass window $M_{H^\pm} - M_{H_2}$ depends on $\cos(\beta-\alpha)$, α_b and α_c (the amount of *CPV* admixture in H_2 and H_3), the window is usually only 80–250 GeV wide. There is lower bound on $M_{H^\pm} > 650$ GeV as required by *B* physics. Thus our analysis restricts $M_{H^\pm}$, for a given choice of parameters, both from above and below.

(vii) Our plots also show how, increasing the value for α_c the two heavier Higgs bosons flip from "mostly *CP*-even" to "mostly *CP*-odd". And while the dominant decay is into $t\bar{t}$, the decays into bosonic states are next largest and can be used to distinguish this scenario.

In conclusion, our work shows that the parameter space of the *CPV* 2HDM is very constrained, and the neutral Higgs bosons in the *CPV* type-II 2HDM show some interesting features, which could distinguish them from Higgs bosons in other models at the colliders.

ACKNOWLEDGMENTS

The work of M. F. has been partly supported by NSERC through the Grant No. SAP105354. M. T. would like to thank FRQNT for financial support under Grant No. PRC-290000.

[1] A. Pich, The standard model of electroweak interactions, Report No. CERN-2012-001.

[2] C. Furey, $SU(3)_C \times SU(2)_L \times U(1)_Y (\times U(1)_X)$ as a symmetry of division algebraic ladder operators, Eur. Phys. J. C **78**, 375 (2018).

[3] R. A. Diaz, R. Martinez, and F. Ochoa, The scalar sector of the SU(3)(c) x SU(3)(L) x U(1)(X) model, Phys. Rev. D **69**, 095009 (2004).

[4] S. F. Novaes, Standard model: An introduction, in *Proceedings of the 10th Jorge Andre Swieca Summer School*

on Particle and Fields (World Scientific, Singapore, 2000), pp. 5–102, arXiv:hep-ph/0001283.
[5] H. E. Logan, TASI 2013 lectures on Higgs physics within and beyond the Standard Model, arXiv:1406.1786.
[6] ATLAS Collaboration, Observation of a new particle in the search for the Standard Model Higgs boson with the ATLAS detector at the LHC, Phys. Lett. B **716**, 1 (2012).
[7] CMS Collaboration, Observation of a new boson at a mass of 125 GeV with the CMS Experiment at the LHC, Phys. Lett. B **716**, 30 (2012).
[8] J. D. Lykken, Beyond the standard model, CERN Yellow Report No. CERN-2010-002, pp. 101–109, 2010, http://lss.fnal.gov/archive/2010/conf/fermilab-conf-10-103-t.pdf.
[9] J. F. Gunion, H. E. Haber, G. L. Kane, and S. Dawson, *The Higgs Hunter's Guide* (Addison-Wesley, Boston, Massachusetts, 2000), Vol. 80; H. E. Haber and G. L. Kane, The search for supersymmetry: Probing physics beyond the standard model, Phys. Rep. **117**, 75 (1985); J. F. Gunion and H. E. Haber, Higgs bosons in supersymmetric models (I), Nucl. Phys. **B272**, 1 (1986); **B402**, 567(E) (1993).
[10] G. C. Branco, P. M. Ferreira, L. Lavoura, M. N. Rebelo, M. Sher, and J. P. Silva, Theory and phenomenology of two-Higgs-doublet models, Phys. Rep. **516**, 1 (2012).
[11] H. P. Nilles, Supersymmetry, supergravity and particle physics, Phys. Rep. **110**, 1 (1984).
[12] E. Accomando *et al.*, Workshop on *CP* studies and non-standard Higgs physics, Report No. CERN-2006-009.
[13] A. Pilaftsis and C. E. M. Wagner, Higgs bosons in the minimal supersymmetric standard model with explicit *CP* violation, Nucl. Phys. **B553**, 3 (1999).
[14] H. E. Haber and D. O'Neil, Basis-independent methods for the two-Higgs-doublet model. II. The significance of $\tan\beta$, Phys. Rev. D **74**, 015018 (2006).
[15] A. Sakharov, Violation of *CP* Invariance, C asymmetry, and baryon asymmetry of the universe, Sov. Phys. Usp. **34**, 392 (1991).
[16] V. Kuzmin, V. Rubakov, and M. Shaposhnikov, On the anomalous electroweak baryon number nonconservation in the early universe, Phys. Lett. **155B**, 36 (1985).
[17] J. F. Gunion and H. E. Haber, The *CP* conserving two Higgs doublet model: The approach to the decoupling limit, Phys. Rev. D **67**, 075019 (2003).
[18] H. E. Haber and O. Stål, New LHC benchmarks for the $\mathcal{CP}$ -conserving two-Higgs-doublet model, Eur. Phys. J. C **75**, 491 (2015).
[19] B. Grzadkowski, O. Ogreid, and P. Osland, Testing the presence of *CP* violation in the 2HDM, Proc. Sci., CORFU2014 (**2015**) 086.
[20] V. Keus, S. F. King, S. Moretti, and K. Yagyu, *CP* violating two-Higgs-doublet model: Constraints and LHC predictions, J. High Energy Phys. 04 (2016) 048.
[21] N. Darvishi and M. Krawczyk, *CP* violation in the extension of SM with a complex singlet scalar and vector quarks, Nucl. Phys. **B962**, 115 (2021).
[22] D. Emmanuel-Costa, O. Ogreid, P. Osland, and M. Rebelo, *CP* violation in the scalar sector, Proc. Sci., CORFU2015 (**2016**) 044.
[23] A. Pich and P. Tuzon, Yukawa alignment in the two-Higgs-doublet model, Phys. Rev. D **80**, 091702 (2009).
[24] A. Arhrib, E. Christova, H. Eberl, and E. Ginina, *CP* violation in charged Higgs production and decays in the complex two Higgs doublet model, J. High Energy Phys. 04 (2011) 089.
[25] M. Jung, A. Pich, and P. Tuzon, Charged-Higgs phenomenology in the aligned two-Higgs-doublet model, J. High Energy Phys. 11 (2010) 003.
[26] S.-S. Bao, Y. Tang, and Y.-L. Wu, $W^{\pm}H^{\mp}$ associated production at LHC in the general 2HDM with spontaneous *CP* violation, Phys. Rev. D **83**, 075006 (2011).
[27] L. Basso, A. Lipniacka, F. Mahmoudi, S. Moretti, P. Osland, G. Pruna, and M. Purmohammadi, Probing the charged Higgs boson at the LHC in the *CP*-violating type-II 2HDM, J. High Energy Phys. 11 (2012) 011.
[28] M. Jung and A. Pich, Electric dipole moments in two-Higgs-doublet models, J. High Energy Phys. 04 (2014) 076.
[29] J. Brod, U. Haisch, and J. Zupan, Constraints on *CP*-violating Higgs couplings to the third generation, J. High Energy Phys. 11 (2013) 180.
[30] S. Inoue, M. J. Ramsey-Musolf, and Y. Zhang, *CP*-violating phenomenology of flavor conserving two Higgs doublet models, Phys. Rev. D **89**, 115023 (2014).
[31] R. Gaitán, J. H. Montes de Oca, E. A. Garcés, and R. Martinez, Rare top decay $t \to c\gamma$ with flavor changing neutral scalar interactions in two Higgs doublet model, Phys. Rev. D **94**, 094038 (2016).
[32] C.-Y. Chen, S. Dawson, and Y. Zhang, Complementarity of LHC and EDMs for exploring Higgs *CP* violation, J. High Energy Phys. 06 (2015) 056.
[33] S. L. Glashow and S. Weinberg, Natural conservation laws for neutral currents, Phys. Rev. D **15**, 1958 (1977).
[34] H. Georgi and D. V. Nanopoulos, Suppression of flavor changing effects from neutral spinless meson exchange in gauge theories, Phys. Lett. **82B**, 95 (1979).
[35] V. D. Barger, J. L. Hewett, and R. J. N. Phillips, New constraints on the charged Higgs sector in two Higgs doublet models, Phys. Rev. D **41**, 3421 (1990).
[36] Y. Grossman, Phenomenology of models with more than two Higgs doublets, Nucl. Phys. **B426**, 355 (1994).
[37] A. G. Akeroyd, Nonminimal neutral Higgs bosons at LEP-2, Phys. Lett. B **377**, 95 (1996).
[38] A. Djouadi, The anatomy of electroweak symmetry breaking. II. The Higgs bosons in the minimal supersymmetric model, Phys. Rep. **459**, 1 (2008).
[39] D. A. Demir, Effects of the supersymmetric phases on the neutral Higgs sector, Phys. Rev. D **60**, 055006 (1999).
[40] S. Y. Choi, M. Drees, and J. S. Lee, Loop corrections to the neutral Higgs boson sector of the MSSM with explicit *CP* violation, Phys. Lett. B **481**, 57 (2000).
[41] M. Carena, J. R. Ellis, A. Pilaftsis, and C. E. M. Wagner, Renormalization group improved effective potential for the MSSM Higgs sector with explicit *CP* violation, Nucl. Phys. **B586**, 92 (2000).
[42] M. Carena, J. R. Ellis, A. Pilaftsis, and C. E. M. Wagner, Higgs boson pole masses in the MSSM with explicit *CP* violation, Nucl. Phys. **B625**, 345 (2002).

[43] S. King, M. Muhlleitner, R. Nevzorov, and K. Walz, Exploring the *CP*-violating NMSSM: EDM constraints and phenomenology, Nucl. Phys. **B901**, 526 (2015).
[44] S. Y. Choi and J. S. Lee, MSSM Higgs boson production at hadron colliders with explicit *CP* violation, Phys. Rev. D **61**, 115002 (2000).
[45] S. Y. Choi, K. Hagiwara, and J. S. Lee, Higgs boson decays in the minimal supersymmetric standard model with radiative Higgs sector *CP* violation, Phys. Rev. D **64**, 032004 (2001).
[46] S. Y. Choi, M. Drees, J. S. Lee, and J. Song, Supersymmetric Higgs boson decays in the MSSM with explicit *CP* violation, Eur. Phys. J. C **25**, 307 (2002).
[47] J. S. Lee, Manifestations of *CP* violation in the MSSM Higgs sector, AIP Conf. Proc. **1078**, 36 (2009).
[48] P. Bechtle, O. Brein, S. Heinemeyer, O. Stål, T. Stefaniak, G. Weiglein, and K. E. Williams, HiggsBounds-4: Improved tests of extended Higgs sectors against exclusion bounds from LEP, the Tevatron and the LHC, Eur. Phys. J. C **74**, 2693 (2014).
[49] S. Kraml, T. Q. Loc, D. T. Nhung, and L. D. Ninh, Constraining new physics from Higgs measurements with LILITH: Update to LHC Run 2 results, SciPost Phys. **7**, 052 (2019).
[50] D. Fontes, M. Mühlleitner, J. C. Romão, R. Santos, J. a. P. Silva, and J. Wittbrodt, The C2HDM revisited, J. High Energy Phys. 02 (2018) 073.
[51] CMS Collaboration, A measurement of the Higgs boson mass in the diphoton decay channel, Phys. Lett. B **805**, 135425 (2020).
[52] M. Mühlleitner, M. O. Sampaio, R. Santos, and J. Wittbrodt, ScannerS: Parameter scans in extended scalar sectors, Eur. Phys. J. C **82**, 198 (2022).
[53] J. Bernon and B. Dumont, LILITH: A tool for constraining new physics from Higgs measurements, Eur. Phys. J. C **75**, 440 (2015).
[54] A. Djouadi and G. Moreau, The couplings of the Higgs boson and its *CP* properties from fits of the signal strengths and their ratios at the $7 + 8$ TeV LHC, Eur. Phys. J. C **73**, 2512 (2013).
[55] I. F. Ginzburg and M. Krawczyk, Symmetries of two Higgs doublet model and *CP* violation, Phys. Rev. D **72**, 115013 (2005).
[56] M. Bertrand, S. Kraml, T. Q. Loc, D. T. Nhung, and L. D. Ninh, Constraining new physics from Higgs measurements with LILITH-2, Proc. Sci., TOOLS2020 (**2021**) 040.
[57] B. W. Kernighan and D. M. Ritchie, *International Edition c Programming Language*, 2nd ed. (Englewood Cliffs NJ Prentice Hall, Hoboken, New Jersey, 1988).
[58] B. Stroustrup, *The c++ Programming Language*, 4th ed. (Addison-Wesley, Boston, Massachusetts, 2013), p. 1360.
[59] R. Brun and F. Rademakers, Root-an object oriented data analysis framework, Nucl. Instrum. Methods Phys. Res., Sect. A **389**, 81 (1997).
[60] P. Bechtle, S. Heinemeyer, O. Stal, T. Stefaniak, and G. Weiglein, Applying exclusion likelihoods from LHC searches to extended Higgs sectors, Eur. Phys. J. C **75**, 421 (2015).
[61] HFLAV Collaboration, Averages of b-hadron, c-hadron, and τ-lepton properties as of 2018, Eur. Phys. J. C **81**, 226 (2021).
[62] S. Antusch, O. Fischer, A. Hammad, and C. Scherb, Testing *CP* properties of extra Higgs states at the HL-LHC, J. High Energy Phys. 03 (2021) 200.
[63] M. Baak, M. Goebel, J. Haller, A. Hoecker, D. Kennedy, R. Kogler, K. Mönig, M. Schott, and J. Stelzer, The electroweak fit of the standard model after the discovery of a new boson at the LHC, Eur. Phys. J. C **72**, 2205 (2012).
[64] T. Enomoto and R. Watanabe, Flavor constraints on the two Higgs doublet models of Z_2 symmetric and aligned types, J. High Energy Phys. 05 (2016) 002.
[65] Particle Data Group, Review of particle physics, Prog. Theor. Exp. Phys. **2020**, 083C01 (2020).
[66] G. Funk, D. O'Neil, and R. M. Winters, What the oblique parameters S, T, and U and their extensions reveal about the 2HDM: A numerical analysis, Int. J. Mod. Phys. A **27**, 1250021 (2012).
[67] W. Grimus, L. Lavoura, O. M. Ogreid, and P. Osland, A precision constraint on multi-Higgs-doublet models, J. Phys. G **35**, 075001 (2008).
[68] T. Abe, J. Hisano, T. Kitahara, and K. Tobioka, Gauge invariant Barr-Zee type contributions to fermionic EDMs in the two-Higgs doublet models, J. High Energy Phys. 01 (2014) 106.
[69] D. Bowser-Chao, D. Chang, and W.-Y. Keung, Electron Electric Dipole Moment from *CP* Violation in the Charged Higgs Sector, Phys. Rev. Lett. **79**, 1988 (1997).
[70] S. M. Barr and A. Zee, Electric Dipole Moment of the Electron and of the Neutron, Phys. Rev. Lett. **65**, 21 (1990).
[71] E. J. Chun, J. Kim, and T. Mondal, Electron EDM and muon anomalous magnetic moment in two-Higgs-doublet models, J. High Energy Phys. 12 (2019) 068.
[72] W. Altmannshofer, S. Gori, N. Hamer, and H. H. Patel, Electron EDM in the complex two-Higgs doublet model, Phys. Rev. D **102**, 115042 (2020).
[73] L. Wang, J. M. Yang, M. Zhang, and Y. Zhang, Revisiting lepton-specific 2HDM in light of muon $g-2$ anomaly, Phys. Lett. B **788**, 519 (2019).
[74] E. J. Chun, The muon $g-2$ in two-Higgs-doublet models, EPJ Web Conf. **118**, 01006 (2016).
[75] L. Wang and X.-F. Han, A light pseudoscalar of 2HDM confronted with muon $g-2$ and experimental constraints, J. High Energy Phys. 05 (2015) 039.
[76] A. Broggio, E. J. Chun, M. Passera, K. M. Patel, and S. K. Vempati, Limiting two-Higgs-doublet models, J. High Energy Phys. 11 (2014) 058.
[77] V. Ilisie, New Barr-Zee contributions to $(g-2)_\mu$ in two-Higgs-doublet models, J. High Energy Phys. 04 (2015) 077.
[78] T. Abe, R. Sato, and K. Yagyu, Lepton-specific two Higgs doublet model as a solution of muon $g-2$ anomaly, J. High Energy Phys. 07 (2015) 064.
[79] C.-Y. Chen, H.-L. Li, and M. Ramsey-Musolf, *CP*-violation in the two Higgs doublet model: From the LHC to EDMs, Phys. Rev. D **97**, 015020 (2018).
[80] ACME Collaboration, Improved limit on the electric dipole moment of the electron, Nature (London) **562**, 355 (2018).

[81] A. Mendez and A. Pomarol, Signals of *CP* violation in the Higgs sector, Phys. Lett. B **272**, 313 (1991).
[82] W. Bernreuther and A. Brandenburg, Tracing *CP* violation in the production of top quark pairs by multiple TeV proton proton collisions, Phys. Rev. D **49**, 4481 (1994).
[83] O. M. Ogreid, P. Osland, and M. N. Rebelo, *CP* violation in extended Higgs sectors, Proc. Sci., CORFU2017 (**2018**) 044.
[84] I. F. Ginzburg, M. Krawczyk, and P. Osland, Resolving SM like scenarios via Higgs boson production at a photon collider. 1. 2HDM versus SM, arXiv:hep-ph/0101208.
[85] P. M. Ferreira, R. Guedes, J. F. Gunion, H. E. Haber, M. O. P. Sampaio, and R. Santos, The *CP*-conserving 2HDM after the 8 TeV run, in *Proceedings of the 22nd International Workshop on Deep-Inelastic Scattering and Related Subjects* (2014), arXiv:1407.4396.
[86] E. Accomando, D. Englert, J. Hays, and S. Moretti, Voyage across the 2HDM Type-II with Magellan, arXiv:1905.07313.
[87] ATLAS Collaboration, Measurements of the Higgs boson inclusive and differential fiducial cross-sections in the diphoton decay channel with pp collisions at $\sqrt{s} =$ 13 TeV with the ATLAS detector, arXiv:2202.00487.
[88] ATLAS Collaboration, Constraints on Higgs boson production with large transverse momentum using $H \to b\bar{b}$ decays in the ATLAS detector, Phys. Rev. D **105**, 092003 (2022).
[89] ATLAS Collaboration, Measurements of the Higgs boson inclusive and differential fiducial cross sections in the 4ℓ decay channel at $\sqrt{s}=13$TeV, Eur. Phys. J. C **80**, 942 (2020).
[90] N. Chen, T. Han, S. Su, W. Su, and Y. Wu, Type-II 2HDM under the precision measurements at the Z-pole and a Higgs factory, J. High Energy Phys. 03 (2019) 023.
[91] I. F. Ginzburg and I. P. Ivanov, Tree-level unitarity constraints in the most general 2HDM, Phys. Rev. D **72**, 115010 (2005).
[92] B. Grinstein, C. W. Murphy, and P. Uttayarat, One-loop corrections to the perturbative unitarity bounds in the *CP*-conserving two-Higgs doublet model with a softly broken $\mathbb{Z}_2$ symmetry, J. High Energy Phys. 06 (2016) 070.
[93] V. Cacchio, D. Chowdhury, O. Eberhardt, and C. W. Murphy, Next-to-leading order unitarity fits in two-Higgs-doublet models with soft $\mathbb{Z}_2$ breaking, J. High Energy Phys. 11 (2016) 026.
[94] R. V. Harlander, S. Liebler, and H. Mantler, SusHi: A program for the calculation of Higgs production in gluon fusion and bottom-quark annihilation in the standard model and the MSSM, Comput. Phys. Commun. **184**, 1605 (2013).
[95] A. Djouadi, J. Kalinowski, and M. Spira, HDECAY: A program for Higgs boson decays in the standard model and its supersymmetric extension, Comput. Phys. Commun. **108**, 56 (1998).
[96] A. Djouadi, J. Kalinowski, M. Muehlleitner, and M. Spira, HDECAY: Twenty$_{++}$ years after, Comput. Phys. Commun. **238**, 214 (2019).
[97] K. Yagyu, Studies on extended Higgs sectors as a probe of new physics beyond the standard model, Ph.D. thesis, Toyama University, 2012.
[98] S. Kanemura, Y. Okada, E. Senaha, and C. P. Yuan, Higgs coupling constants as a probe of new physics, Phys. Rev. D **70**, 115002 (2004).
[99] J. M. Butterworth *et al.*, The Tools and Monte Carlo Working Group Summary Report from the Les Houches 2009 Workshop on TeV Colliders, in *Proceedings of the 6th Les Houches Workshop on Physics at TeV Colliders* (2010), arXiv:1003.1643.
[100] ATLAS Collaboration, Search for heavy ZZ resonances in the $\ell^+\ell^-\ell^+\ell^-$ and $\ell^+\ell^-\nu\bar{\nu}$ final states using proton–proton collisions at $\sqrt{s} = 13$ TeV with the ATLAS detector, Eur. Phys. J. C **78**, 293 (2018).
[101] CMS Collaboration, Measurements of properties of the Higgs boson in the four-lepton final state at $\sqrt{s} = 13$ TeV, Report No. CMS-PAS-HIG-18-001, (CERN, Geneva, 2018)https://cds.cern.ch/record/2621419?ln=en.
[102] CMS Collaboration, Measurements of properties of the Higgs boson decaying into four leptons in pp collisions at $\sqrt{s} = 13$ TeV, Report No. CMS-PAS-HIG-19-001.
[103] L. Cosmai and M. Consoli, Experimental signals for a second resonance of the Higgs field, Int. J. Mod. Phys. A **37**, 2250091 (2022).
[104] S. Antusch, O. Fischer, A. Hammad, and C. Scherb, Explaining excesses in four-leptons at the LHC with a double peak from a *CP* violating two Higgs doublet model, arXiv:2112.00921.